Analysis of Phasor Distortions by Fog in Time-of-Flight Measurement

Keita Yamazaki

Graduate School of Library, Information and Media Studies

University of Tsukuba

March 2020

Analysis of Phasor Distortions by Fog in Time-of-Flight Measurement
Time-of-Flight 計測における霧による距離計測歪みの解析

Student No.: 201821638
Name: Keita Yamazaki

This thesis proposes a time-of-flight (ToF) measurement method that can estimate the depth in a foggy scene. It is known that depth measurement by ToF camera in a foggy scene cannot capture correct phase difference and amplitude. This is because the light emitted from the light source of the ToF camera is scattered by the fog, and the optical path length of the light returning from the target object is different from that without the fog. This study uses a ray-tracing simulation to reveal the change in ToF measurement value when light is scattered by fog and adversely affects the measurement. This thesis examines the following parameters: the distance between the object and the ToF camera, the modulation frequency of the illumination emitted from the light source of the ToF camera, and the scattering coefficient of the fog. Based on the results, this thesis creates a look-up table that estimates the depth from the ToF measurement value of the scene with fog. The effectiveness of the proposed method was evaluated for unknown scenes in the simulation.

Academic Advisors: Principal: Yoichi OCHIAI
Secondary: Norihiko UDA

Contents

List of Figures

Chapter 1

Introduction

The study of distance measurement in computer vision plays an essential role in implementing automated driving technology, and accurate distance information to people, other vehicles, and obstacles around the vehicle is required. Various measurement and sensor modalities have been researched and developed to realize the above tasks. One of the major challenges in distance measurement is that measurement methods provide incorrect distance information even in weather conditions and environments that are sufficiently visible to humans, such as light fog and underwater. Time-of-Flight (ToF) cameras used for distance measurement, are known to produce erroneous measurement results because the reflected light from the target, which should have been obtained, is added to the light scattered by the fog [2, 3, 4, 5, 6].

Our experiments verify that information about amplitude and phase in the ToF measurement results changes depending on the scattering, based on the ToF renderer's results [1]. This study will construct a lookup table based on the rendering results to extract depth information from the scene measurement results with distractors and verify whether correct depth can be obtained.

Our main contributions in this study can be summarized as follows:

- Investigation of the tendency of ToF measurements to be distorted in the presence of scatterers (chapters 5 and 7, appendix A).
- Creation a look-up table for depth estimation in scenes with scatterers (chapter 5).
- Confirmation of the effectiveness of the proposed method using simulation experiments (chapter 6).

This thesis consists of eight chapters. Chapter 2 describes previous studies in computer vision dealing with scenes with scattering and clarifies the position of this research. Chapter 3 describes the method and principle of ToF measurement. Chapter 4 describes the phasor representations and phasor distortions. Chapter 5 describes the verification of phasor distortions in scenes with scatterers using the ToF renderer [1]. In addition, this chapter describes a depth estimation method using a look-up table. In chapter 6, the discussion of this study is presented. In Chapter 7, the discussion of this study is presented. Chapter 8 is a summary.

Chapter 2

Related Work

In computer vision, analyzing scenes where fog-like scattering occurs has been an important research topic. This chapter introduces related work on scattering and clarifies the position of this study by classifying it into three types of scene analysis methods: *removing effects of scattering* (section 2.1), *scene analysis using effects of scattering* (section 2.2), and *scene analysis without effects of scattering* (section 2.3).

2.1 Removing effects of scattering

The presence of scattering agents in a scene, such as fog, muddy water, or rain, has a significant impact on the measurement results of cameras and other sensors, even when the weather and environment are sufficiently visible to humans. Methods for removing scattering effects in the scene and sharpening the image have been proposed to address this problem. Methods for removing the effects of scattering and analyzing a scene can be classified into two categories: methods using *RGB cameras and algorithms* (section 2.1.1), and methods using *special hardware and algorithms* (section 2.1.2).

2.1.1 RGB camera and algorithms

Typical examples of methods using *RGB cameras and algorithms* are He et al. [7], Berman et al. [8], Cai et al. [9], Narasimhan et al. [10].

He et al. [7] proposed a method called *Dark Channel Prior*. This method focuses on the lowest value in the subregion of the captured image to remove the effect of fog. Berman et al. [8] proposed a method to remove scattering effects, noting that in scenes with fog, lines called *haze-line* are formed in RGB space when the same color is placed at different locations. In these methods, the effect of scattering is removed from the image based on color information, but since the image is obscured by scattering, there is a problem that the accuracy varies depending on the scene being photographed.

Cai et al. [9] proposed a method to remove the effects of scattering such as fog using a folding neural network, a deep learning method. A problem with deep learning methods is that they are dependent on the training data, and it is difficult to explain how accurate the depth estimate can be.

Narasimhan et al. [10] proposed a method to remove the effect of scattering from an image based on both user input and image information.

2.1.2 Special hardware and algorithms

The method of *special hardware and algorithms* includes the ToF camera method [2, 3, 4, 5, 6], the projector method [11], the projector and camera array method [12], and the RGB camera and light detection and ranging (LiDAR) sensor fusion method [13]. Gupta et al. [2] proposed a ToF measurement method that is robust to multi-path interference problems such as inter-reflections by using a phasor imaging to represent the value measured by a ToF camera. Muraji et al. [3, 4, 5] proposed a ToF measurement method that is unaffected by fog by performing ToF measurement at multiple modulation frequencies. Suzuki et al. [6] designed a ToF measurement method that is not affected by fog, noting that the measured values of each reflectance vary due to the effect of the fog.

Narasimhan et al. [11] used structured illumination to remove scattering effects, and Levoy et al. [12] proposed a synthetic aperture method to remove scattering within the range of turbid water. Also, a method was proposed to remove the effect of scattering by fusing measurement information from the RGB camera and LiDAR [13].

2.2 Scene analysis using effects of scattering

2.2.1 RGB camera and algorithms

Rahadianti et al. [14] build a neural network that establishes a correlation between the scattering effect in an image and the depth of a scene and propose a method to estimate the depth of a scene using the scattering in the scene. Rahadianti et al. [15] also proposed a method to obtain the distance from the camera to the object from the image intensity of the scatterer.

Berman et al. [8] proposed a method that removes the effects of scattering and estimates the distance to the object from the effects of fog.

2.2.2 Special hardware and algorithms

A stereo camera is a method that can acquire depth information of a scene, but when scatterers such as fog are present, the contrast of the image becomes low, and the features of the image become ambiguous, making stereo matching difficult. Therefore, Li et al. [16] and Caraffa et al. [17] proposed a method to obtain the depth information of a scene using the fog thickness as a cue.

Although it does not deal with fog, a method to classify materials by photographing scatterers using a ToF camera has also been proposed [18].

2.3 Scene analysis without effects of scattering

Unlike the above two methods, RGB camera is always affected by scattering, so there is currently no method that uses RGB camera and algorithms without being affected by scattering in principle.

In terms of research that falls under the category of methods using *special hardware and algorithms*, methods using millimeter-wave radar [19, 20, 21], sensor fusion of LiDAR and millimeter-wave radar [22], methods using polarization [23, 24], and methods using infrared

light have been proposed [25, 26]. In recent years, quantum radar cameras [27, 28], ToF cameras that can remove backscatter and reflections [29], methods that use line sensors and line lasers to remove backscatter [30], and Single Photon Avalanche Diode (SPAD) cameras have been proposed [31].

2.4 Position of this study

While these methods are well-studied, previous studies on scattering are classified as *removing effects of scattering* and *special hardware and algorithms*, as shown in Table 2.1. Inspired by the work of Muraji et al. [3, 4, 5], this study uses the ToF renderer [1] to investigate the distortion trend of ToF measurements in scenes with scattering. Based on the trend, a lookup table is created, and depth measurement is performed.

Table 2.1: Table of related work.

	RGB camera and algorithms	Special hardware and algorithms
Removing effects of scattering	He+09 [7] Berman+16 [8] Cai+16 [9] Narasimhan+03 [10]	ToF Camera Gupta+15 [2], Muraji+18,19 [3, 4, 5], Suzuki+18 [6] **Proposed Method** RGB Camera + Projector : Narasimhan+05 [11] Projector + Camera Array : Levoy+04 [12] RGB Camera + LiDAR : Bijelic+19 [13]
Scene analysis using effects of scattering	Berman+16 [8] Rahadianti+17 [14] Rahadianti+17 [15]	Stereo Camera : Li+15 [16], Caraffa+13 [17] ToF Camera : Tanaka+17 [18]
Scene analysis without effects of scattering		MMW Rader : Appleby+07 [19], Pencikowski+96 [20], Sweet+96 [21] MMW Rader + LiDAR : Ryde+09 [22] Polarization : Walker+00 [23], Schehner+01 [24] Infra-red : Jingyun+16 [25], Viitanen+14 [26] Quantum Rader : Hirota+16 [27, 28] ToF Camera : Tadano+15 [29] Line Sensor + Line Laser : Wang+18 [30] SPAD : Satat+18 [31]

Chapter 3

Time-of-Flight Measurement

This chapter explains the measurement principle of the ToF camera used in this study, using the Mitsuba Renderer [32], a physically-based renderer, and the Mitsuba ToF Renderer [1], a Time-of-Flight renderer-enabled version of the Mitsuba Renderer.

3.1 The measurement principle of ToF camera

A ToF camera is a device that measures the time it takes for the light emitted from the light source to be reflected by the object and returned to the camera. There are two types of ToF measurement methods: the direct ToF method and the indirect ToF method [33]. This study assumes that the amplitude-modulated continuous wave (AMCW) camera, which is a type of indirect ToF method, is used.

The AMCW ToF camera used in this study can measure the distance and the reflectance information of the object. In a ToF camera, the amplitude-modulated sine wave is irradiated to the object as a scene incident wave to be measured. Then, the reflected wave reflected from the object and returned to the camera is compared with a reference wave of the same waveform as the incident wave. The amplitude and phase of the reflected wave is measured as shown in Figure 3.1. The amplitude of the reflected wave becomes the reflectance information of the object, and the phase becomes the distance to the object. The amplitude $a(f, x)$ and phase $\phi(f, d(x))$ of an object at a distance $d(x)$ measured by each pixel of the AMCW ToF camera are expressed by the following equation, as given by [3]:

$$\begin{cases} a(f,x) & = r(x) \\ \phi(f,d(x)) & = \frac{4\pi f d(x)}{c} \end{cases} \tag{3.1}$$

where f is the modulation frequency of the AMCW ToF camera, x is the position of pixel, r is the amplitude and c is the speed of light (3.00×10^8 m/s).

3.2 Recovery of amplitude and phase at a single modulation frequency in a ToF renderer [1]

A cross-correlation is necessary to mathematically recover amplitude and phase from the reflected wave acquired by a ToF camera using the AMCW method [34]. Real ToF cameras can be used without being aware of cross-correlation by application programming interfaces

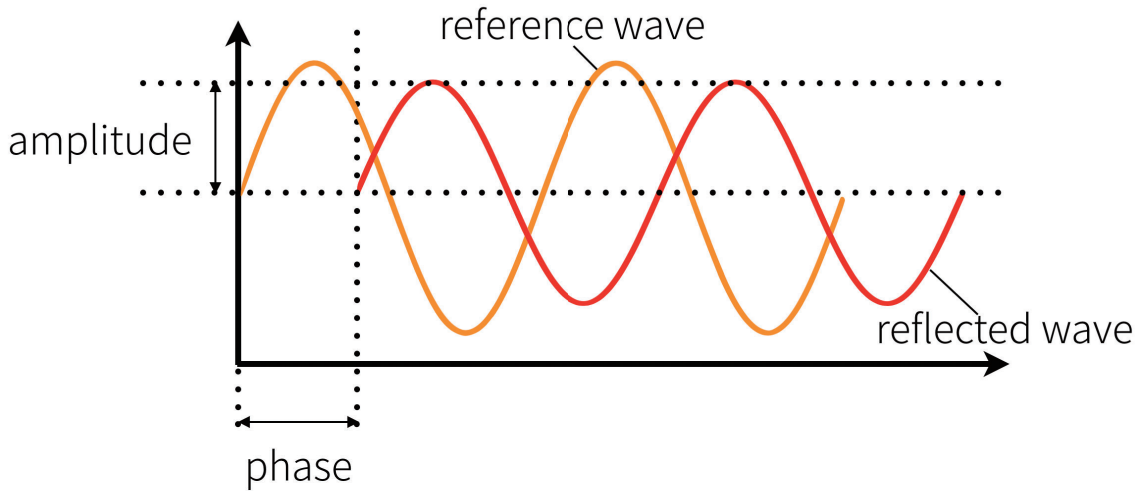

Figure 3.1: Measurement principle of the AMCW ToF camera. (Prepared with reference to [3].)

and software development kits provided by developers. However, ToF Renderer [1] needs to be aware of cross-correlation. Specifically, the phase of the amplitude-modulated sine wave used as the incident wave and reference wave of the scene is changed at 90° intervals, as shown in Figure 3.2. The amplitude a and phase ϕ can be recovered by combining images of the scene taken at 90-degree intervals. Figure 3.3 shows images of a scene taken when the modulation frequency is set to 600 kHz. This study uses a 3D model of a Cornell Box[1] adapted to ToF rendering. The image taken when the phase of the sine wave is set to 0° is $c(\tau_0)$, the image taken when the phase is changed by 90° is $c(\tau_{90})$, the image taken when the phase is changed to 180° is $c(\tau_{180})$, and the image taken when the phase is changed to 270° is $c(\tau_{270})$. The following equations are used to recover amplitude a and phase ϕ from these images [34] :

$$a = \frac{\sqrt{[c(\tau_{270}) - c(\tau_{90})]^2 + [c(\tau_0) - c(\tau_{180})]^2}}{2} \tag{3.2}$$

$$\phi = \tan^{-1}\left(\frac{c(\tau_{270}) - c(\tau_{90})}{c(\tau_0) - c(\tau_{180})}\right). \tag{3.3}$$

Figure 3.4 shows an image from which the amplitude and phase was recovered from Figure 3.3. Based on the recovered phase, the distance d_e can be estimated by the following equation [34]:

$$d_e = \frac{c}{2f} \times \frac{\phi}{2\pi}. \tag{3.4}$$

An example of the image with depth estimation is shown in Figure 3.5.

3.3 ToF measurement using multiple modulation frequencies

In the AMCW camera, if a measurement is made with only a single modulation frequency, the phase is between 0 and 2 π, and each measurement remains undetermined by 2 π. Therefore, the AMCW ToF camera uses multiple modulation frequencies to perform the

[1] http://www.graphics.cornell.edu/online/box/

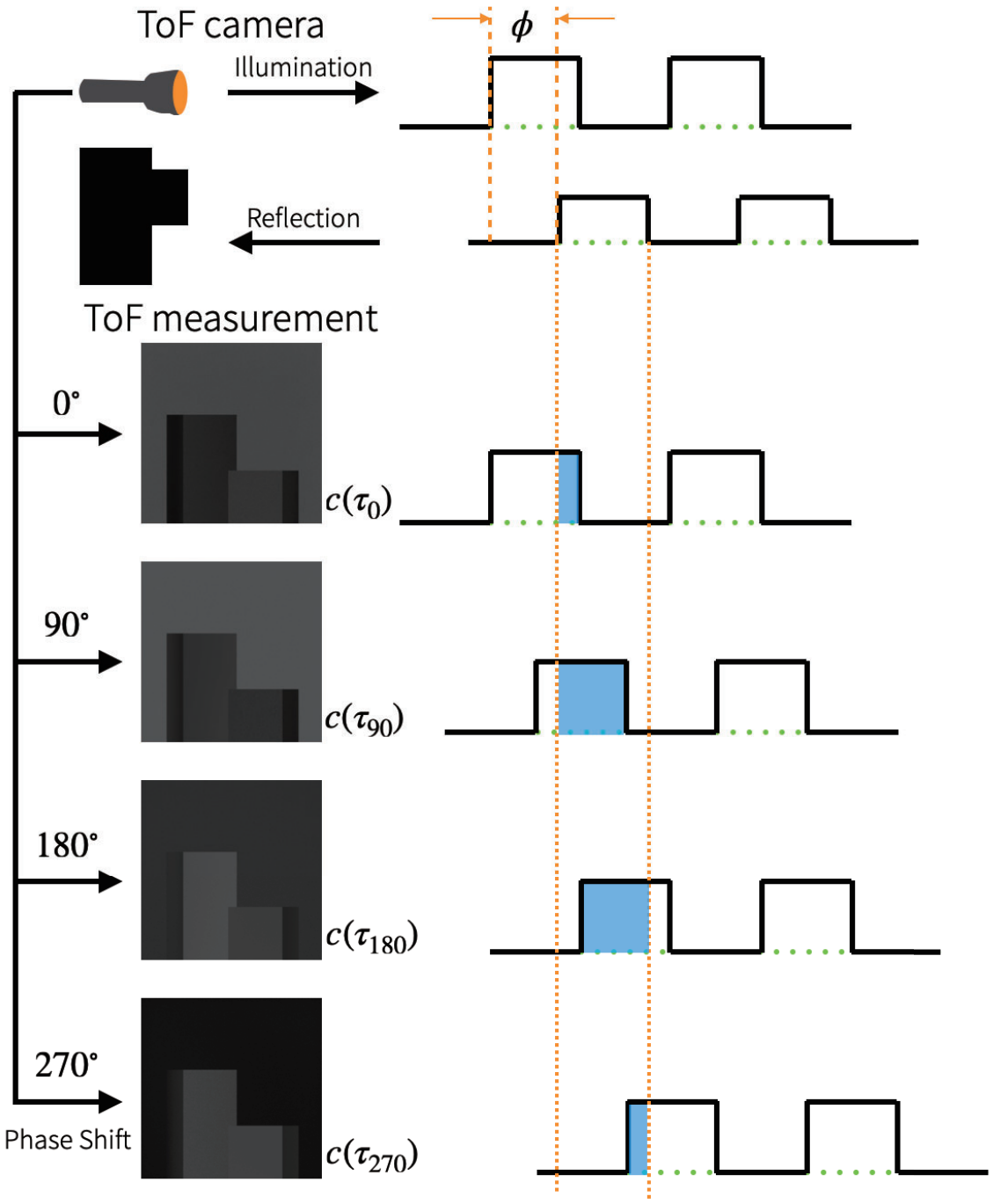

Figure 3.2: Amplitude and phase recovery by phase shift of reference wave. (Prepared with reference to [34].)

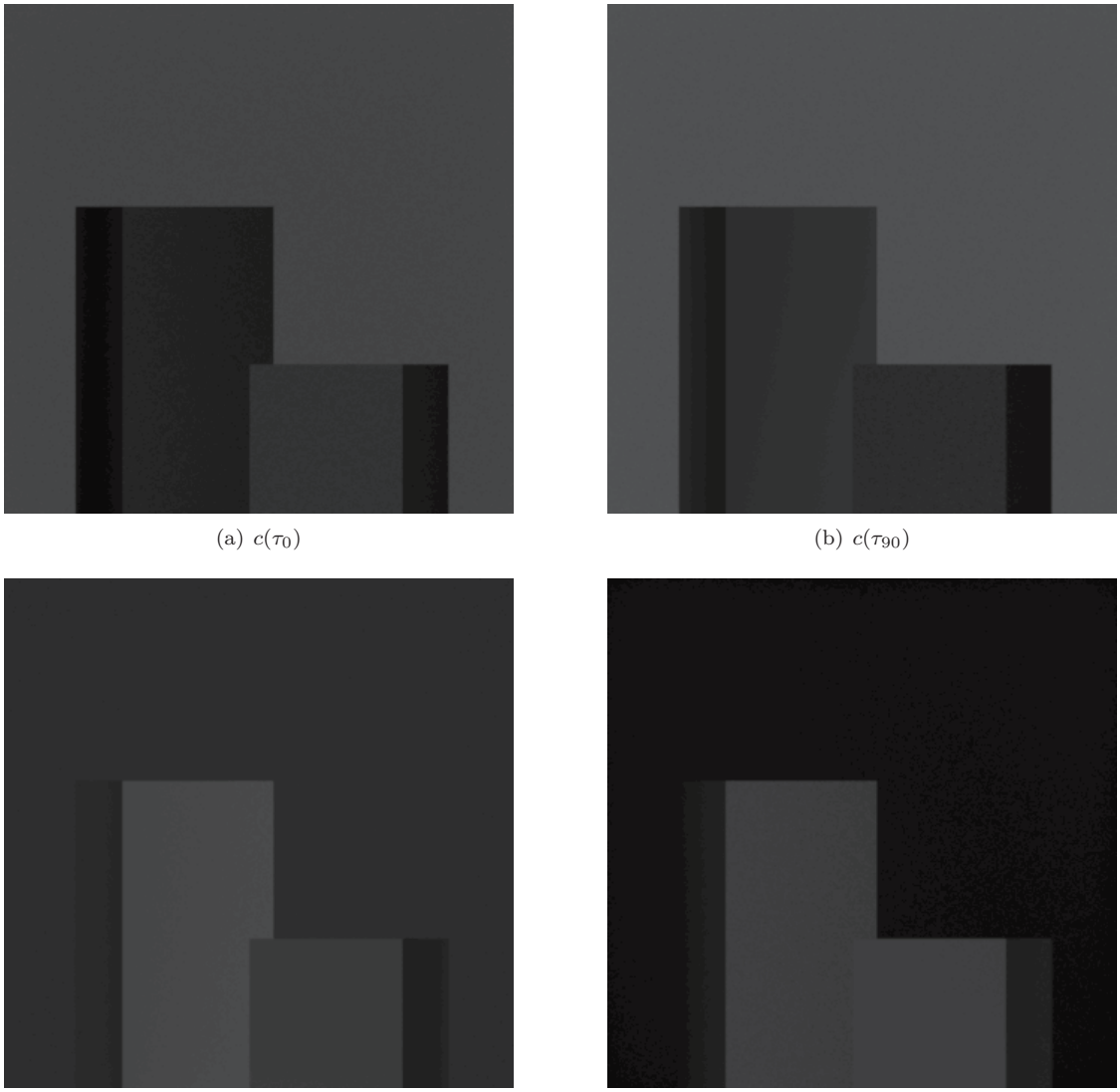

(a) $c(\tau_0)$ (b) $c(\tau_{90})$

(c) $c(\tau_{180})$ (d) $c(\tau_{270})$

Figure 3.3: The resulting image of ToF rendering when the modulation frequency is set to 600 kHz.

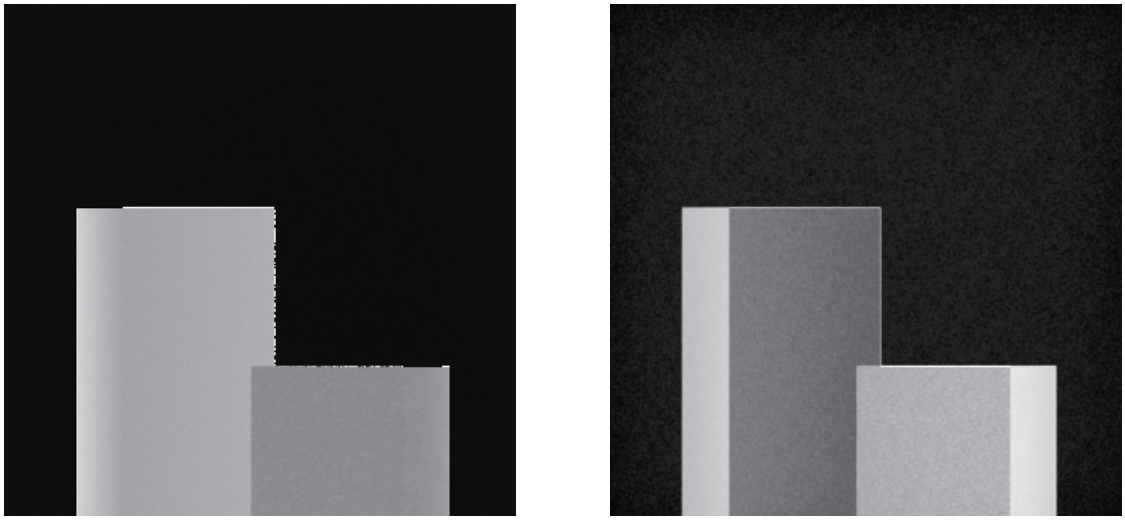

(a) The phase image

(b) The amplitude image

Figure 3.4: Image with amplitude and phase recovered.

Figure 3.5: Single frequency depth estimation image.

(a) Depth estimation image using multiple modulation frequencies.

(b) True value image

Figure 3.6: Depth estimation using multiple frequencies.The modulation frequencies used varied from 200 kHz to 1.1 MHz, with 10 modulation frequencies used in increments of 100 kHz.

measurement. According to [3], the amplitude $a(f, x)$ and the phase $\phi(f, d(x))$ of an object at a distance $d(x)$, measured by each pixel x of the AMCW ToF camera, are expressed with the following equations under specific modulation frequencies f_1 and f_2:

$$\begin{cases} a(f_1, x) & = a(f_2, x) \\ \phi(f_1, x) & = \frac{f_1}{f_2}\phi(f_2, x). \end{cases} \tag{3.5}$$

It is known that the distance $\hat{d_e}$ of the desired scene can be estimated by the following equation, according to [3]:

$$\hat{d_e} = \arg\min_{d} \sum_{k=1}^{m} \left| \phi(f_k, x) - \left(\frac{4\pi f_k d}{x} \mod \pi \right) \right| \tag{3.6}$$

where m is the number of modulation frequencies, and $\phi(f_k, x)$ is the phase measured at the k-th modulation frequency f_k. Results for depth estimation images and truth values using multiple modulation frequencies are shown in Figure 3.6. It can be seen that the results are closer to the true value than depth estimation using a single modulation frequency.

Chapter 4

Phasor Representations and Phasor Distortions

This chapter describes the phasor representations and phasor distortions of the ToF Measurements.

4.1 Phasor representations

In a previous study [2, 3, 4, 5, 6], it is known that the ToF measurements can be represented as a single phasor by using the amplitude and phase measured by the ToF camera as the length and angle, respectively, on the phasor representations as shown in Figure 4.1. This is called the phasor representations of ToF measurements. According to [3], it is known that Eq. (3.1) can be expressed by the following equation using phasor representations:

$$p(f, x) = a(f, x)e^{i\phi(f,d(x))}, \tag{4.1}$$

where $p(f, x) \in \mathbb{C}$ is the phasor.

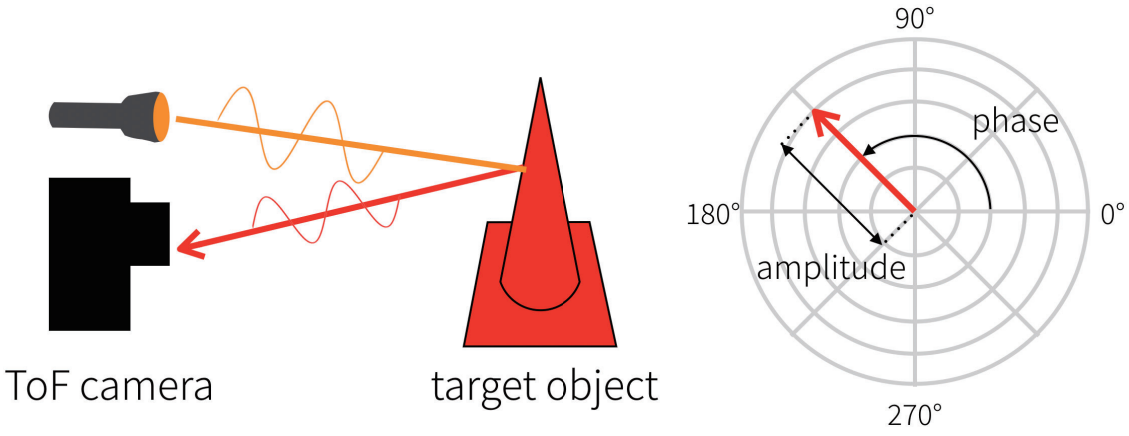

Figure 4.1: Phasor representation of ToF measurement. (Prepared with reference to [3].)

The phasor representation is used to represent two points at the same distance by ToF, which has different amplitude for each reflectance and the same phase, as shown in Figure 4.2.

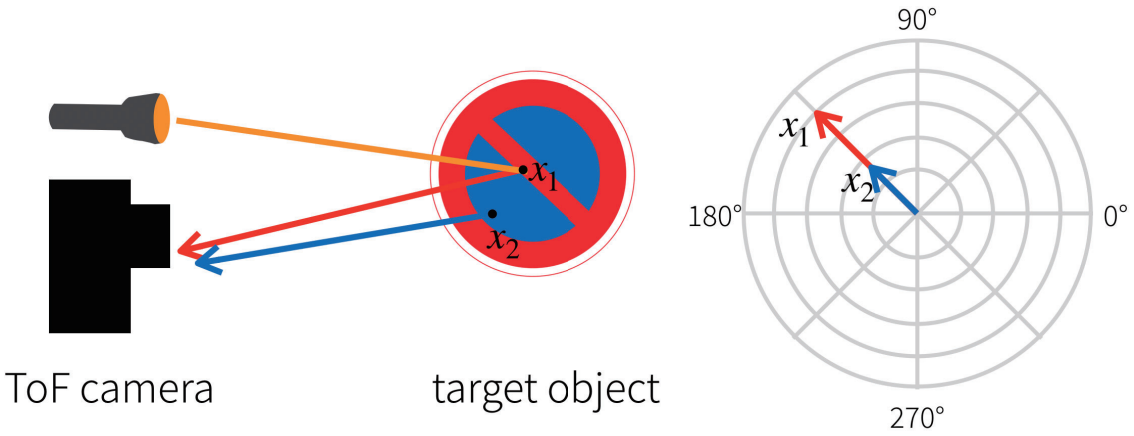

Figure 4.2: Phasor representation of two points at the same distance. (Prepared with reference to [3].)

4.2 Phasor distortions

When a scattering such as fog is present in the scene, amplitude and phase obtained by adding scattered light from the scattering and reflected light directly hitting and returning from the object when ToF measurement is performed becomes the measurement value of the ToF camera [2, 3, 4, 5, 6]. Figure 4.3 shows the results of measuring the scene with and without scattering using the ToF renderer [1]. This confirms that the results are very different depending on the presence or absence of fog. When the phase is used, the surfaces of the object that are recognized as nearly identical in the phase in the scene without fog are treated as entirely different in the scene with fog, which results in erroneous measurement results. From Equation 3.4) and Equation (5.1), since the distance is estimated from the obtained phase, if the phase is different from the true one, the depth is different as well.

When an object at a distance d is measured, the ToF measurement is the sum of the scattering component $p_s \in \mathbb{C}$ from all the scatterers at all the depths and the reflection component $p_t \in \mathbb{C}$ returned directly from the object. According to [3], it is known that the measured value $p(f, x) \in \mathbb{C}$ for a scene with scatterers can be expressed by the following equation:

$$p(f, x) \quad = \quad p_s(f, x) + p_t(f, x). \tag{4.2}$$

As shown in Figure 4.4, light scattering by the scattering distorts both amplitude and phase from the original measurement value, which results in a completely different ToF measurement value. Following [5], this study refers to distortions in measured phase difference caused by scattering as *phasor distortions*.

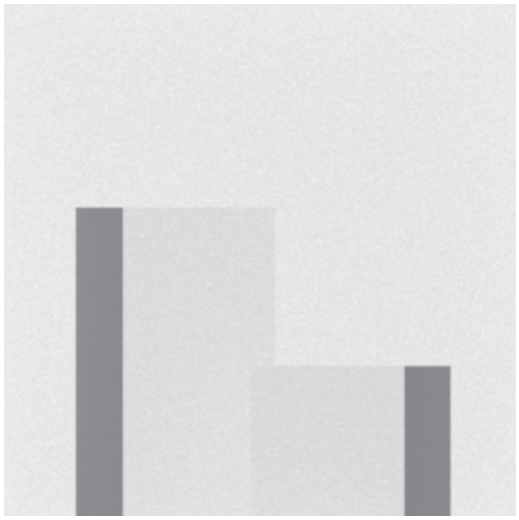

(a) RGB (without fog)

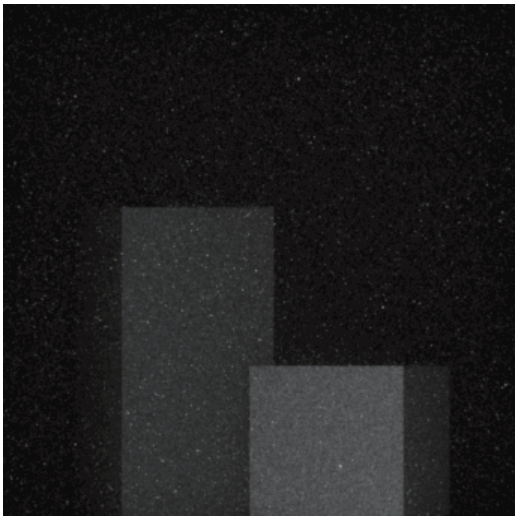

(b) RGB (with fog)

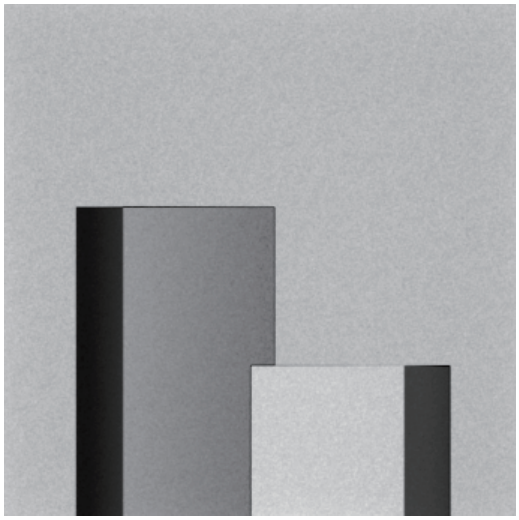

(c) Amplitude (without fog)

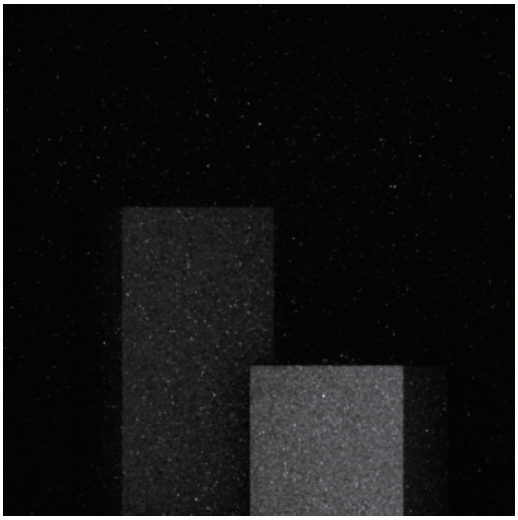

(d) Amplitude (with fog)

(e) Phase (without fog)

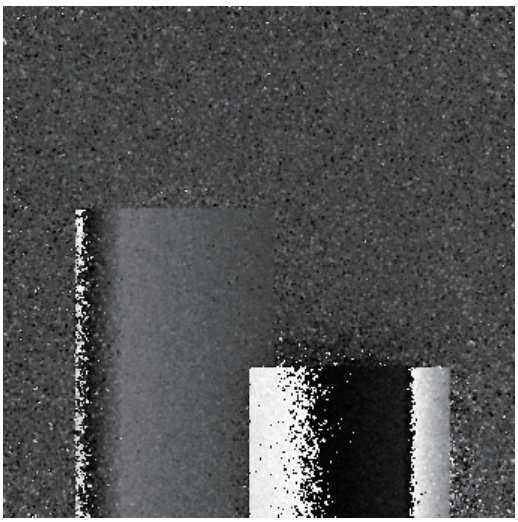

(f) Phase (with fog)

Figure 4.3: Results for different ToF camera measurements with and without fogging. The top row is an RGB image.The middle row is an amplitude image.The bottom row is a phase image.On the left is a scene without fog, and on the right is a scene with fog.It can be seen that the measurement results differ depending on the presence or absence of fog.

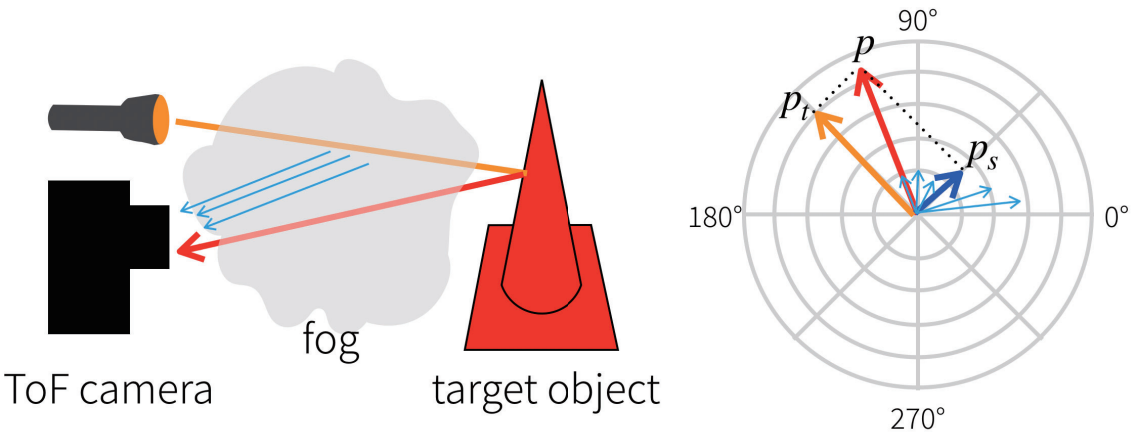

Figure 4.4: Phasor distortions in the fog. Due to the fog scattered light p_s, the value $p = p_s + p_t$ different from the measured value p_t in the scene without fog in both amplitude and phase is obtained. (Prepared with reference to [3].)

Chapter 5

Analysis of Phasor Distortions

This chapter investigates how the phasor is distorted by varying the modulation frequency of a reference wave and the fog scattering coefficient when the distance between an object and a ToF camera is varied, using a ToF renderer for measurement results obtained from ToF measurements of objects in a fog.

5.1 Changing the scattering coefficients of fog

This section examines how the phasor distorts when the fog scatter factor and the distances between the object and the ToF cameras are varied. In this study, the fog scattering coefficients were set to three values: 0.005, 0.01, and 0.02. Figure 5.1 shows a rendered image with the above scatter factor set and a rendered image with a fog-free scene. The 3D model used in this experiment is a resized version of the 3D model available at `http://asura.iaigiri.com/OpenGL/gl15.html` . It can be seen that the greater the value of the fog scattering coefficient, the more the object detail disappears.

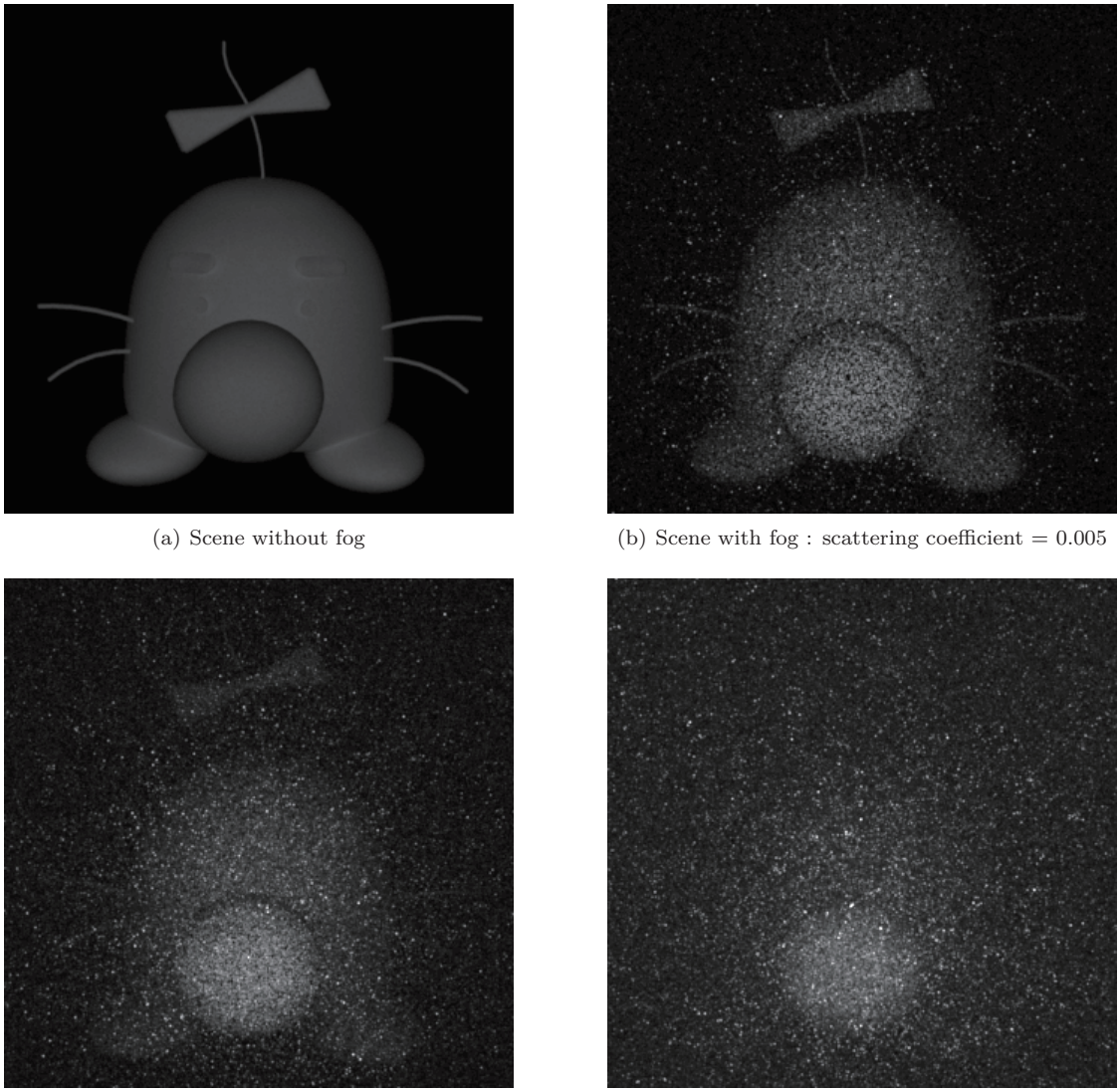

(a) Scene without fog

(b) Scene with fog : scattering coefficient = 0.005

(c) Scene with fog : scattering coefficient = 0.01

(d) Scene with fog : scattering coefficient = 0.02

Figure 5.1: Difference of scene due to change of scattering coefficient. As the scattering coefficient increases, the details of the object disappear.

ToF rendering simulation was used to investigate how the phasor is distorted when the modulation frequency is fixed at 700 kHz, and the scattering coefficient and object position are varied. Their results are shown in Figures. 5.2 and 5.3. In addition, the results of modulation frequencies other than those listed here are attached in the appendix.

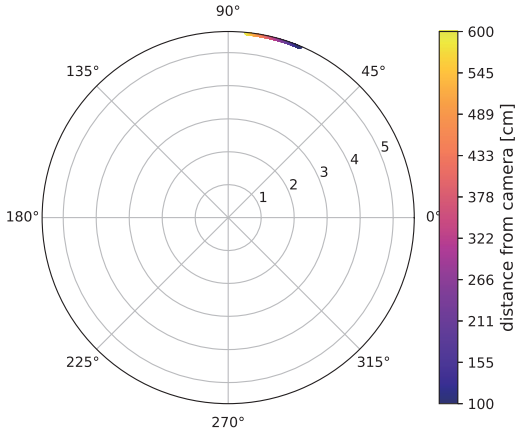

(a) Light reflected from target : scattering coefficient = 0.005

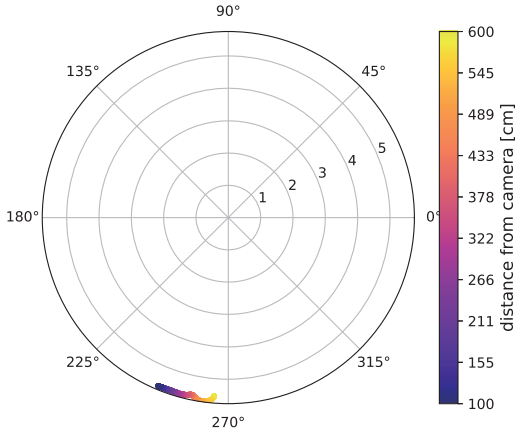

(b) Light scattered by fog : scattering coefficient = 0.005

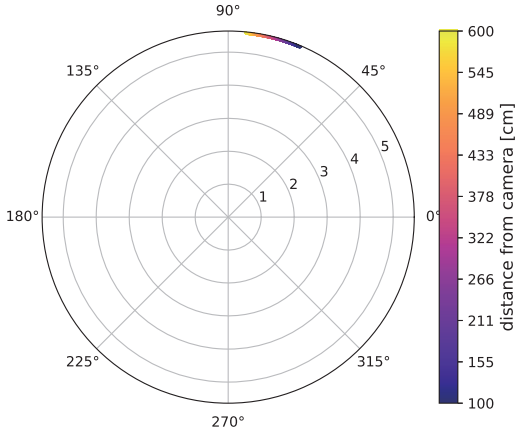

(c) Light reflected from target : scattering coefficient = 0.01

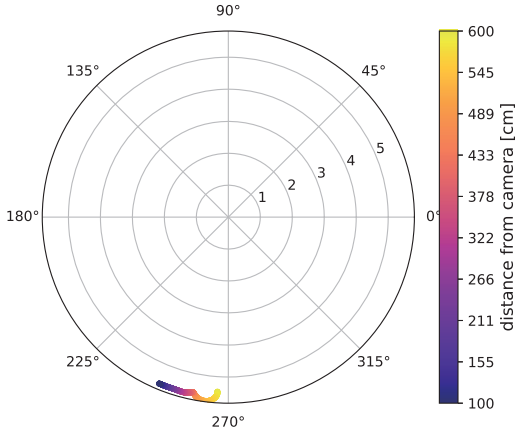

(d) Light scattered by fog : scattering coefficient = 0.01

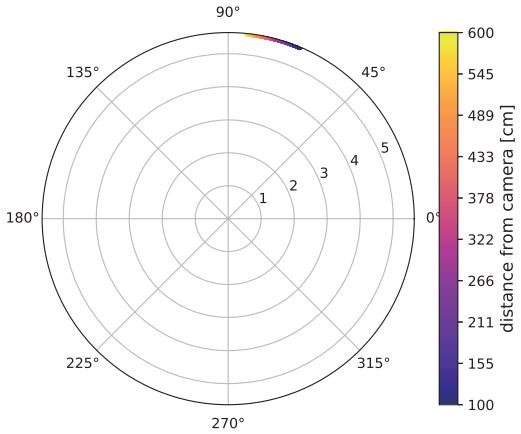

(e) Light reflected from target : scattering coefficient = 0.02

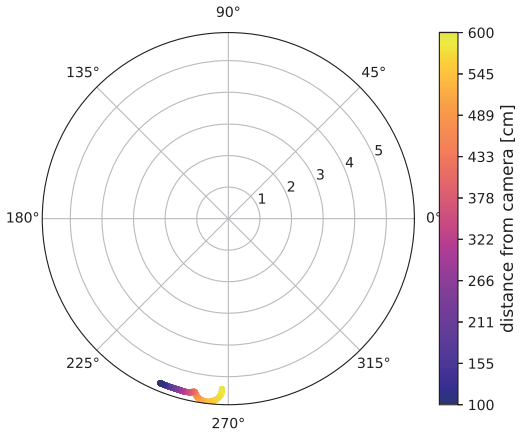

(f) Light scattered by fog : scattering coefficient = 0.02

Figure 5.2: Difference in phasor transition due to difference in scattering coefficient. The upper row is when the scattering coefficient is 0.005. The middle stage is when the scattering coefficient is 0.01. The lower row is when the scattering coefficient is 0.02. The left is the reflected light from the target, and the right is the scattered light due to fog.

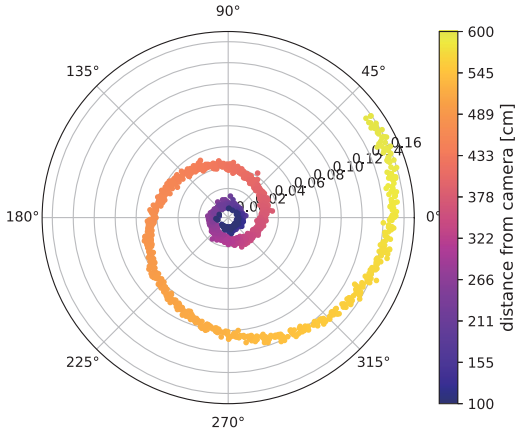

(a) Measured value (scattered light + reflected light) : scattering coefficient = 0.005

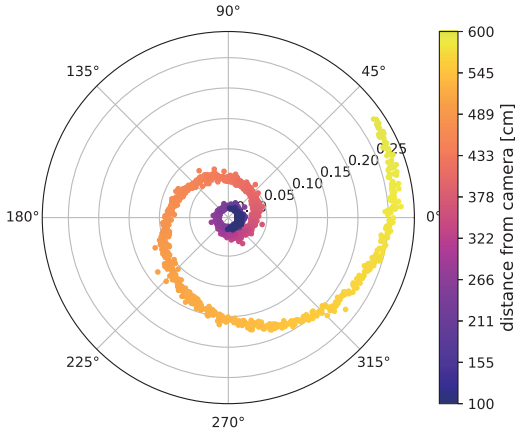

(b) Measured value (scattered light + reflected light) : scattering coefficient = 0.01

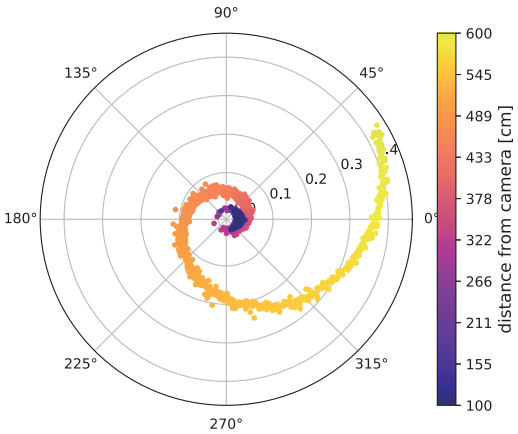

(c) Measured value (scattered light + reflected light) : scattering coefficient = 0.02

Figure 5.3: Difference in phasor transition due to difference in scattering coefficient.

Since the reflected light from the target is a fog-free scene, it can be seen that the amplitude is nearly constant regardless of the scattering coefficient, and the phase changes when the distance of the object changes. Scattered light by fog gradually decreases in amplitude as the scattering coefficient changes. It can also be seen that as the distance of an object moves further, it is more strongly affected by scattering. It can be seen that the measured values have a spiral shape depending on the distance of the object. It can also be seen that the shape of the spiral changes according to the scattering coefficient.

5.2 Changing the modulation frequency of reference wave

This section describes the results of our investigation of how the phasor is distorted when the modulation frequency of the reference wave and the distance between the object and the ToF camera is varied. The scattering coefficients were fixed at 0.005, the modulated frequencies of the reference wave and the distances between the object and the ToF cameras were varied and examined using ToF rendering simulations. These results are shown in Figures. 5.4 and 5.5. The results of the scattering coefficients and modulation frequencies other than those listed here are attached in the appendix.

Like section 5.1, the reflected light from the target has an almost constant amplitude, but as the modulation frequency increases, the greater the distance between the camera and the object, the greater the opening in the phase. It can be seen that the scattered light by fog also has a similar tendency to the reflected light from the target. It can be seen that the larger the value of the modulation frequency, the more the number of turns of the spiral tends to increase.

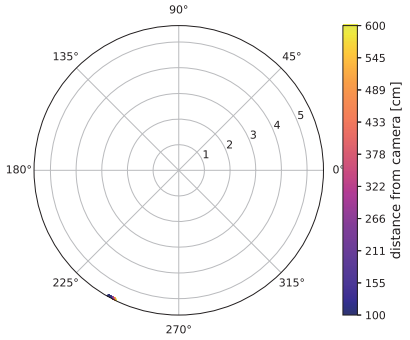

(a) Light reflected from target : modulation frequency = 100 kHz

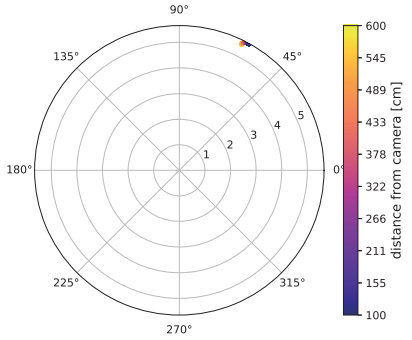

(b) Light scattered by fog : modulation frequency = 100 kHz

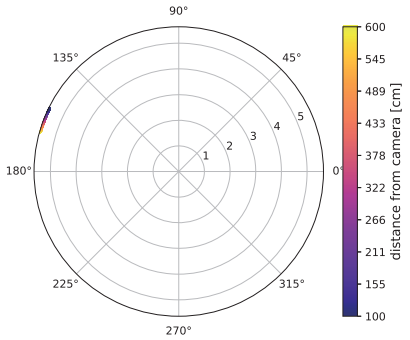

(c) Light reflected from target : modulation frequency = 400 kHz

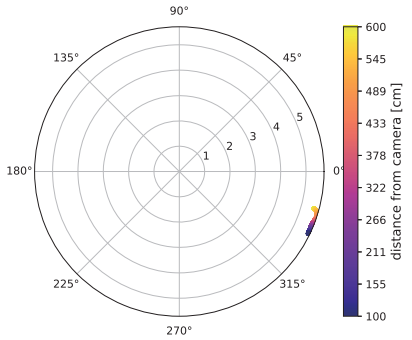

(d) Light scattered by fog : modulation frequency = 400 kHz

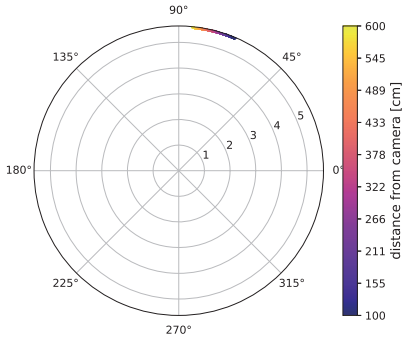

(e) Light reflected from target : modulation frequency = 700 kHz

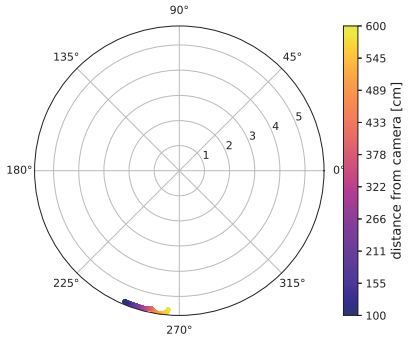

(f) Light scattered by fog : modulation frequency = 700 kHz

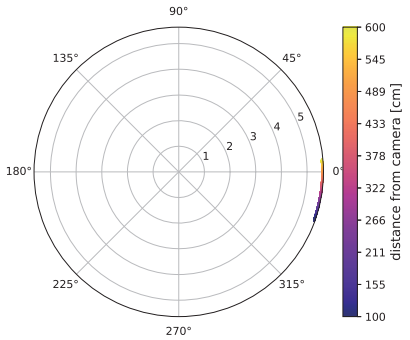

(g) Light reflected from target : modulation frequency = 1 MHz

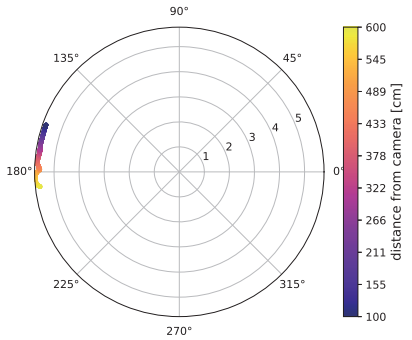

(h) Light scattered by fog : modulation frequency = 1 MHz

Figure 5.4: Difference in phasor transition due to difference in modulation frequency. The scattering coefficient is fixed at 0.005. When the first stage has a modulation frequency of 100 kHz. When the second stage has a modulation frequency of 400 kHz. When the third stage has a modulation frequency of 700 kHz. When the 4th stage is 1 MHz. The left is the reflected light from the target, and the right is the scattered light due to fog.

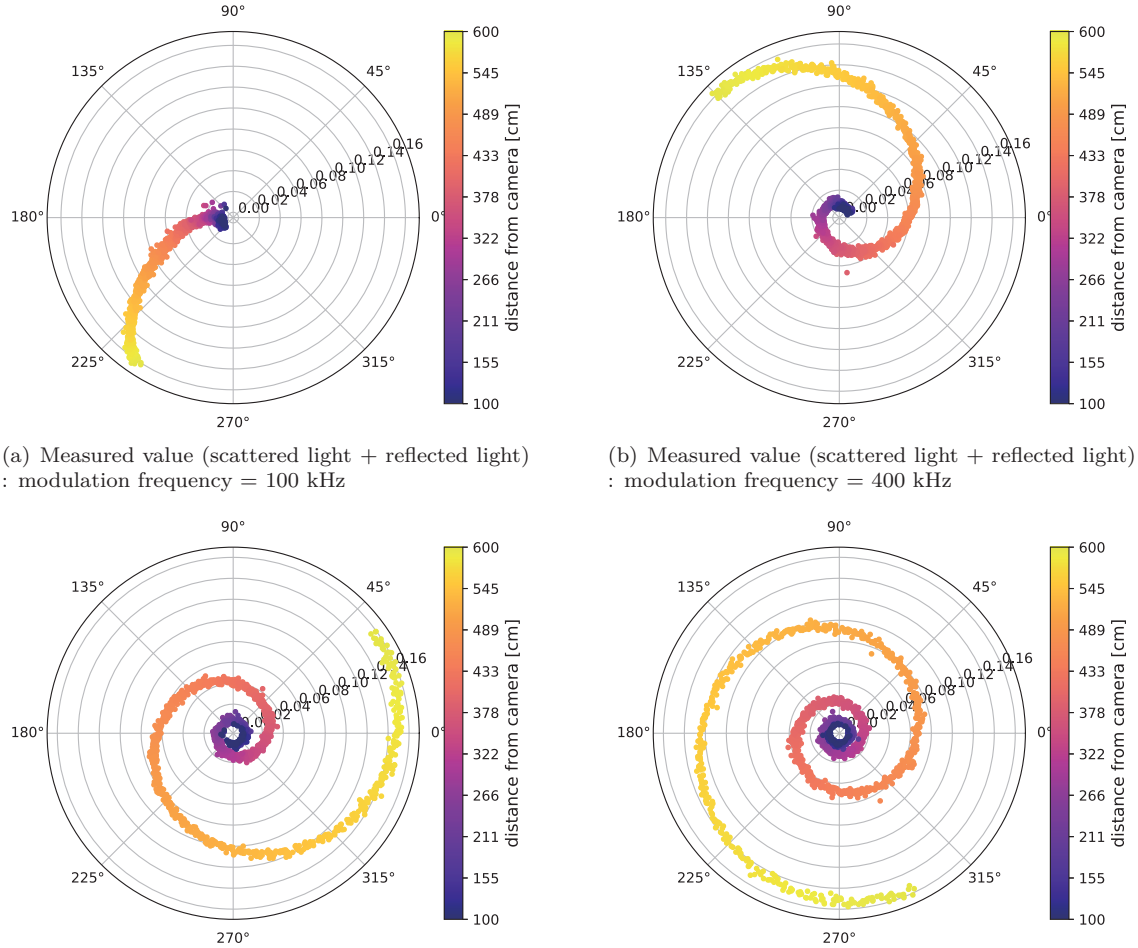

(a) Measured value (scattered light + reflected light) : modulation frequency = 100 kHz

(b) Measured value (scattered light + reflected light) : modulation frequency = 400 kHz

(c) Measured value (scattered light + reflected light) : modulation frequency = 700 kHz

(d) Measured value (scattered light + reflected light) : modulation frequency = 1 MHz

Figure 5.5: Difference in phasor transition due to difference in modulation frequency.

5.3 Depth recovery method

Based on the phasor distortions trends investigated in the previous sections, this section proposes a method for depth estimation by creating a lookup table that estimates depth from phase difference and amplitude in fog. First, in ToF rendering simulations, the modulated frequencies of reference wave, the scattering coefficients of fog, and the positions of cameras and objects are rendered, respectively. From there, phase and amplitude are expressed as phasors, and a look-up table consisting of modulation frequency and phasor, depth value, and scattering coefficient is created.

The distance $\hat{d}$ of an unknown scene with fog is expressed as being the closest distance as a phasor in the look-up table created above:

$$\hat{d} = \arg\min_{d} \sum_{k=1}^{m} |p_t(f_k, d(x), \sigma_s) - p_c(f_k, x)| \tag{5.1}$$

where $p_t(f_k, d(x), \sigma_s) \in \mathbb{C}$ is the phasor corresponding to the depth value $d(x)$ and the fog scatter factor σ s in the k-th modulation frequency f_k, and $p_c(f_k, x) \in \mathbb{C}$ is the phasor

created from the phase and amplitude of the unknown scene measured by the ToF cameras at the k-th modulation frequency f_k.

Chapter 6

Experiments

In order to confirm the usefulness of the method proposed in the section 5.3, one scenes is verified by conducting simulations.

Simulation experiments were conducted on three patterns with fog scattering coefficients of 0.005, 0.01, and 0.02 for the scene where the target object was placed as shown in Figure 6.1(a). Simulations were carried out using parallel light reaching 600 cm ahead. Figures 6.1(b), (c), (d) are scenes where the fog scattering coefficients are 0.005, 0.01, and 0.02, respectively. As the value of the fog scattering coefficient increases, it can be seen that the measurable distance decreases and the detail of the target object is compromised. The results of depth estimation are shown in Figure 6.2. Depth estimation with multiple modulation frequencies by the existing method and depth estimation by the proposed method use a total of 10 types of modulation frequencies per 100 kHz from 100 kHz to 1 MHz.

As shown in Figures 6.2(b), (f), (j), the depth estimation using the conventional method shows that phasor distortion occurs throughout the scene. On the other hand, in the depth estimation using the proposed method shown in Figures 6.2(d), (h), (i), when the fog scattering coefficient increases, the measurable distance becomes shorter, and although it cannot be obtained successfully, it can be seen that the correct distance can be estimated in most parts.

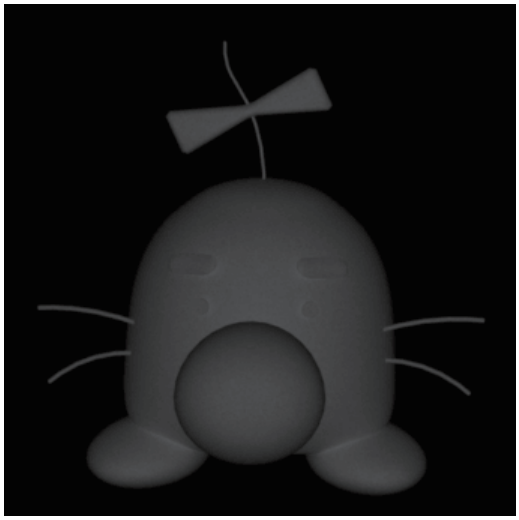

(a) Target scene

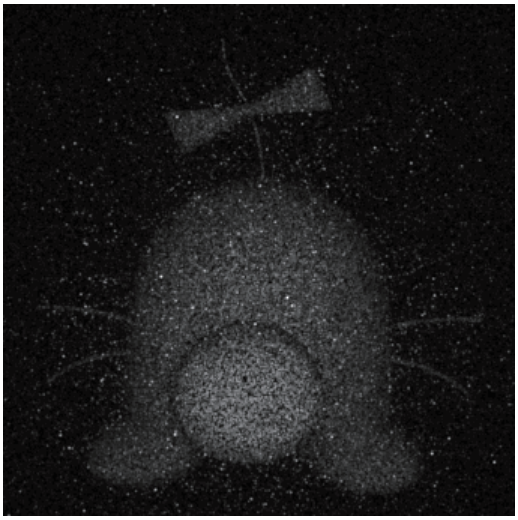

(b) Scene when scattering coefficient = 0.005

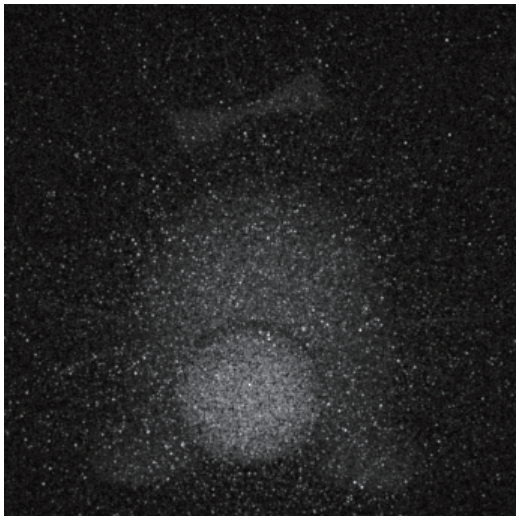

(c) Scene when scattering coefficient = 0.01

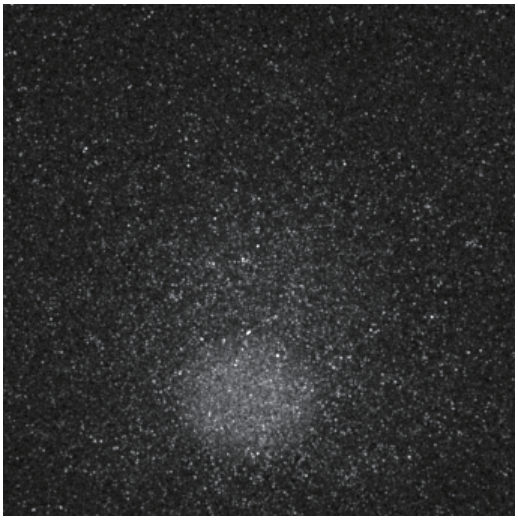

(d) Scene when scattering coefficient = 0.02

Figure 6.1: Experiment environment of scene.

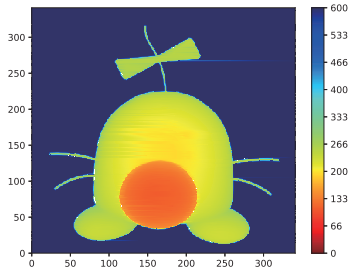

(a) True value

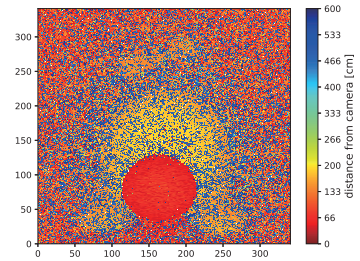

(b) Existing method when scattering coefficient = 0.005

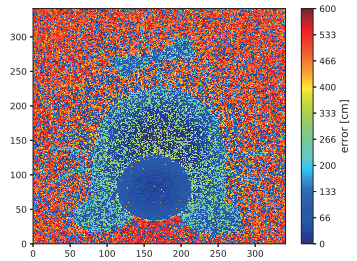

(c) Error between true value and (b)

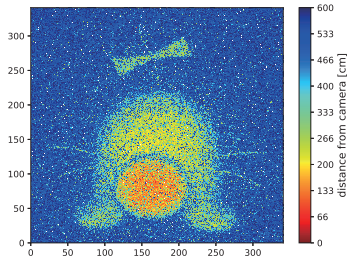

(d) Proposed method when scattering coefficient = 0.005

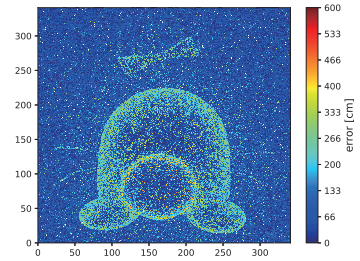

(e) Error between true value and (d)

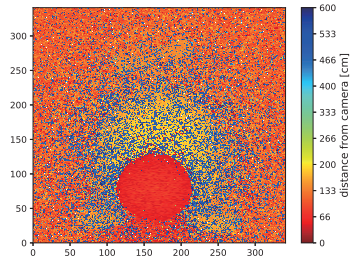

(f) Existing method when scattering coefficient = 0.01

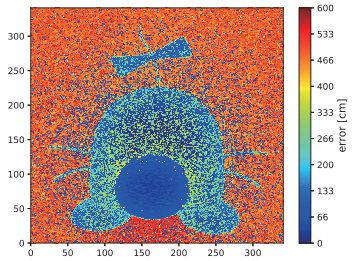

(g) Error between true value and (g)

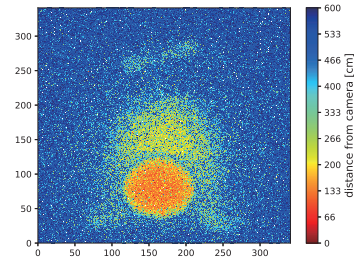

(h) Proposed method when scattering coefficient = 0.01

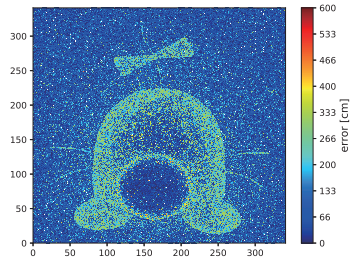

(i) Error between true value and (h)

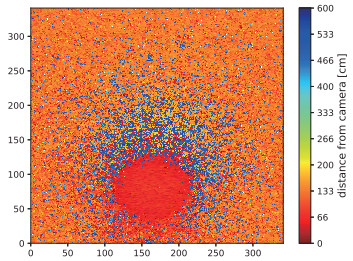

(j) Existing method when scattering coefficient = 0.02

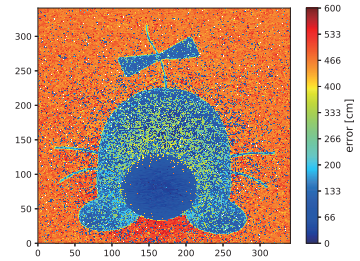

(k) Error between true value and (j)

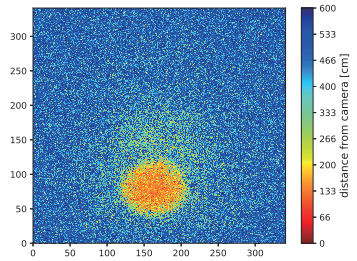

(l) Proposed method when scattering coefficient = 0.02

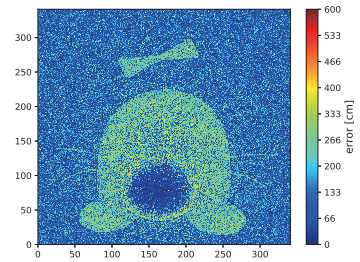

(m) Error between true value and (l)

Figure 6.2: Result of depth estimation.

Chapter 7

Discussion and Future Work

7.1 Discussion

7.1.1 Phasor distortions

The phasor representations of the measured value, shown in the chapter 5 and appendix A, has a spiral transition. The measured value, which is a phasor representation, was converted to Cartesian coordinates. Figure 7.1 shows the phasor transitions in orthogonal coordinates when the fog scatter factor is fixed at 0.005.

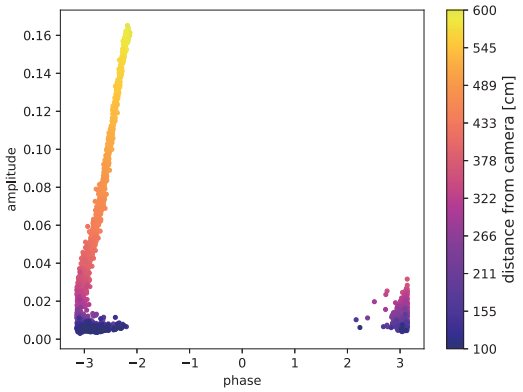

(a) Measured value (scattered light + reflected light) : modulation frequency = 100 kHz

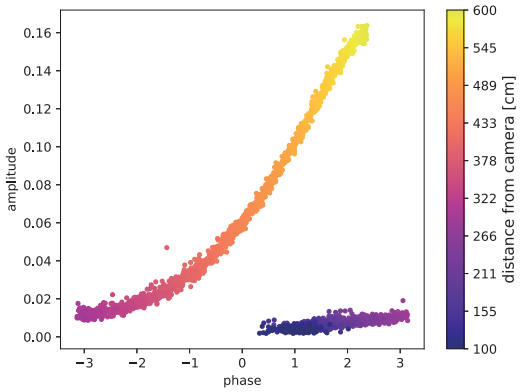

(b) Measured value (scattered light + reflected light) : modulation frequency = 400 kHz

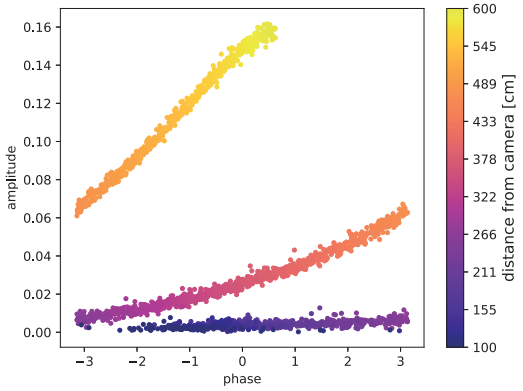

(c) Measured value (scattered light + reflected light) : modulation frequency = 700 kHz

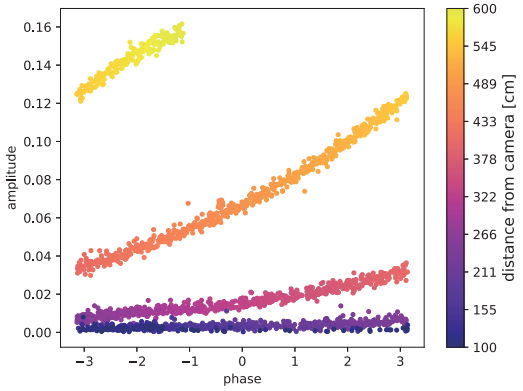

(d) Measured value (scattered light + reflected light) : modulation frequency = 1 MHz

Figure 7.1: Transition of phasor distortion in rectangular coordinates.

Since the diagram is generally similar to a logarithmic function, Figure 7.2 shows the amplitude in Figure 7.1 as a logarithm and transformed into a diagram of orthogonal coordinates.

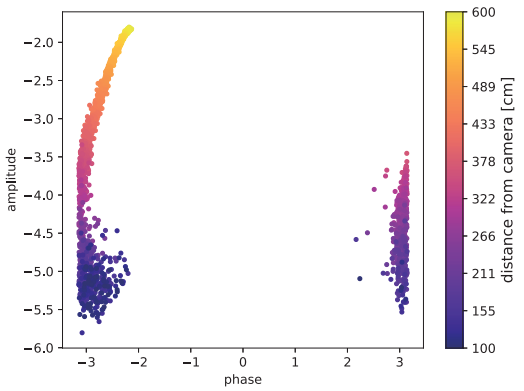

(a) Measured value (scattered light + reflected light) : modulation frequency = 100 kHz

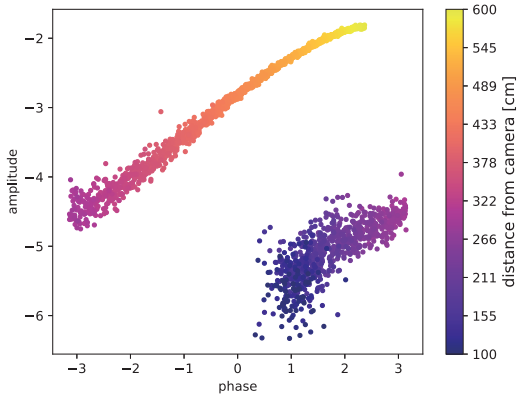

(b) Measured value (scattered light + reflected light) : modulation frequency = 400 kHz

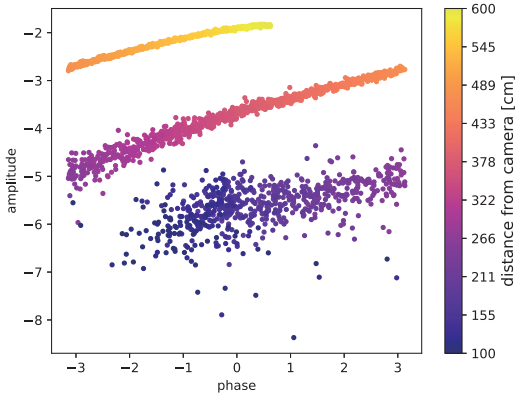

(c) Measured value (scattered light + reflected light) : modulation frequency = 700 kHz

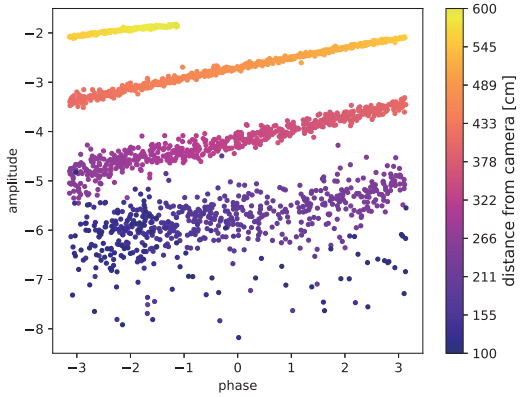

(d) Measured value (scattered light + reflected light) : modulation frequency = 1 MHz

Figure 7.2: Transition of phasor distortion in logarithmic graph.

The logarithmic diagram shows that the phasor transitions are linear. Therefore, it is thought that there is a logarithmic relation between the distances and phasor between cameras and objects. It is believed that there is a logarithmic spiral as a kind of spiral commonly seen in nature, which draws a spiral when displaying polar coordinates and has a logarithmic element, and the distance and phasor between cameras and objects may have a logarithmic spiral relation.

7.1.2 Noise of rendering image

As shown in the image in Figure 6.2, there is a strong particle-like noise. This is because the Monte Carlo Bidirectional Path Tracing used in Mitsuba ToF Renderer [1] is used in simulations.

7.2 Future work

Currently, the usefulness of this method has been confirmed only through simulation. As a prospect, it is necessary to verify the effectiveness of this method by conducting measurements in a real environment. It is not easy to collect data in a real environment to produce a look-up table. Therefore, it is also a future task to consider other methods other than look-up tables. As shown in sections 5.1 and 5.2, the measured phasors varied in spiral shape depending on the scattering coefficient and modulation frequency. This information can be used as a clue for depth estimation methods that do not use look-up tables. For that purpose, it is thought to be necessary to prove theoretically why it spirals like this.

Chapter 8

Conclusion

This thesis investigates the phasor distortions that occurs when performing ToF measurements in foggy scenes, using simulations of ToF imaging to determine how the distortions tends to happen. Based on this tendency, we propose a method for depth estimation by selecting the closest-distance phasor from the measured phasor using a look-up table. To verify the proposed method, experiments are carried out on simulations and the effectiveness is shown. The proposed method produces less true values and errors than the conventional method, and it can be said that the usefulness is higher. However, since the effectiveness of the proposed method is verified only by simulation in this study, it is necessary to verify the usefulness of the method by conducting experiments in the real environment. Also, to create a look-up table, a large amount of data sets are required, and even easy on the simulation, it is severe in the real world. As a future prospect, based on the phasor distortion's transition obtained this time, we believe that we need to devise a method that enables depth estimation without requiring a large amount of data sets.

Acknowledgement

Firstly, I would like to express my appreciation to my thesis advisor Associate Professor Yoichi Ochiai. The donut that Associate Prof. Ochiai gave me during writing my master thesis remains in my impression.

I would like to express my appreciation to Norihiko Uda who is my secondary advisor.

I am also particularity grateful to Assistant Professor Takahito Aoto for constructive suggestions and continuous support. Assistant Prof. Aoto gave me direction on various aspects such as research attitude and programming style. Much appreciated.

I gratefully acknowledge the work of past and present members of our laboratory. Thank you for giving me the wonderful memories.

I would like to thank the secretaries Mineko Matsuse, Rika Matsuoka, and Rumi Okabe for their various support in the laboratory life. Without you, our lab would have been under fire.

Finally, I would like to thank Japan Science and Technology Agency (JST) for a grant that made it possible to complete this study (CREST JPMJCR1781) .

References

[1] Adithya Pediredla, Ashok Veeraraghavan, and Ioannis Gkioulekas. Ellipsoidal Path Connections for Time-Gated Rendering. *ACM Transactions on Graphics*, 38(4):1–12, 2019.

[2] Mohit Gupta, Shree K. Nayar, Matthias B. Hullin, and Jaime Martin. Phasor Imaging: A Generalization of Correlation-Based Time-of-Flight Imaging. *ACM Transactions on Graphics*, 34(5):1–18, 2015.

[3] 連 孟. Time-of-Flight 計測における霧による距離計測歪みの複数の変調周波数を用いた補正. Master's thesis, 奈良先端科学技術大学院大学情報科学研究科, 2019.

[4] 連 孟, 田中 賢一郎, 舩冨 卓哉, 向川 康博. Time-of-Flight 計測における複数の変調周波数を用いた霧による距離計測歪みの補正. 研究報告デジタルコンテンツクリエーション（*DCC*）, 2018-DCC-20(18):1–7, 2018.

[5] Takeshi Muraji, Kenichiro Tanaka, Takuya Funatomi, and Yasuhiro Mukaigawa. Depth from phasor distortions in fog. *Optics Express*, 27(13):18858–18868, 2019.

[6] 鈴木 大介, 田中 賢一郎, 北野 和哉, 舩冨 卓哉, 向川 康博. 極座標系の原点移動モデルを用いた ToF 計測における霧の影響除去. 電子情報通信学会技術研究報告 = *IEICE technical report*, 117(391):293–300, 2018.

[7] Kaiming He, Jian Sun, and Xiaoou Tang. Single image haze removal using dark channel prior. In *Proceedings of IEEE Conference on Computer Vision and Pattern Recognition*, 2009.

[8] Dana Berman, Tali Treibitz, and Shai Avidan. Non-local Image Dehazing. In *Proceedings of IEEE Conference on Computer Vision and Pattern Recognition*, 2016.

[9] Bolun Cai, Xiangmin Xu, Kui Jia, Chunmei Qing, and Dacheng Tao. DehazeNet: An End-to-End System for Single Image Haze Removal. *IEEE Transactions on Image Processing*, 25(11):5187–5198, 2016.

[10] Srinivasa G. Narasimhan and Shree K. Nayar. Interactive Deweathering of an Image using Physical Models. In *Proceedings of ICCV Workshop on Color and Photometric Methods in Computer Vision*, 2003.

[11] Srinivasa G. Narasimhan, Shree K. Nayar, Bo Sun, and Sanjeev J. Koppal. Structured light in scattering media. In *Proceedings of IEEE International Conference on Computer Vision*, 2005.

[12] Marc Levoy, Billy Chen, Vaibhav Vaish, Mark Horowitz, Ian McDowall, and Mark Bolas. Synthetic Aperture Confocal Imaging. *ACM Transactions on Graphics*, 23(3):825–834, 2004.

[13] Mario Bijelic, Fahim Mannan, Tobias Gruber, Werner Ritter, Klaus Dietmayer, and Felix Heide. Seeing Through Fog Without Seeing Fog: Deep Sensor Fusion in the Absence of Labeled Training Data, 2019. `https://arxiv.org/abs/1902.08913`.

[14] Laksmita Rahadianti, Fumihiko Sakaue, and Jun Sato. Depth Estimation for Hazy Images Using Deep Learning. In *Proceedings of IAPR Asian Conference on Pattern Recognition*, 2017.

[15] Laksmita Rahadianti, Wooseong Jeong, Fumihiko Sakaue, and Jun Sato. Time-to-Contact in Scattering Media. *IEICE Transactions on Information and Systems*, E100.D(3):564–573, 2017.

[16] Zhuwen Li, Ping Tan, Robby T. Tan, Danping Zou, Steven Zhiying Zhou, and Loong-Fah Cheong. Simultaneous video defogging and stereo reconstruction. In *Proceedings of IEEE Conference on Computer Vision and Pattern Recognition*, 2015.

[17] Laurent Caraffa and Jean-Philippe Tarel. Stereo Reconstruction and Contrast Restoration in Daytime Fog. In *Proceedings of the Asian conference on Computer Vision*, 2013.

[18] Kenichiro Tanaka, Yasuhiro Mukaigawa, Takuya Funatomi, Hiroyuki Kubo, Yasuyuki Matsushita, and Yasushi Yagi. Material Classification Using Frequency-and Depth-Dependent Time-of-Flight Distortion. In *Proceedings of IEEE Conference on Computer Vision and Pattern Recognition*, 2017.

[19] Roger Appleby and Rupert N. Anderton. Millimeter-Wave and Submillimeter-Wave Imaging for Security and Surveillance. *Proceedings of the IEEE*, 95(8):1683–1690, 2007.

[20] Paul S. Pencikowski. Low-cost vehicle-mounted enhanced vision system comprised of a laser illuminator and range-gated camera. In *Proceedings of Enhanced and Synthetic Vision*, 1996.

[21] Barbara T. Sweet and Carlo L.M. Tiana. Image processing and fusion for landing guidance. In *Proceedings of Enhanced and Synthetic Vision*, 1996.

[22] Julian Ryde and Nick Hillier. Performance of laser and radar ranging devices in adverse environmental conditions. *Journal of Field Robotics*, 26(9):712–727, 2009.

[23] John G. Walker, Peter C. Y. Chang, and Keith I. Hopcraft. Visibility depth improvement in active polarization imaging in scattering media. *Applied Optics*, 39(27):4933–4941, 2000.

[24] Yoav Y. Schechner, Srinivasa G. Narasimhan, and Shree K. Nayar. Instant dehazing of images using polarization. In *Proceedings of IEEE Conference on Computer Vision and Pattern Recognition*, 2001.

[25] Zhang Jingyun, Ding Yifan, Yang Yi, and Sun Jiasong. Real-time defog model based on visible and near-infrared information. In *Proceedings of IEEE International Conference on Multimedia Expo Workshops*, 2016.

[26] J. Viitanen, P. Pyykönen, and R. Täppinen. Active infrared illumination in fog for driver assistance. In *Proceedings of IEEE International Conference on Intelligent Computer Communication and Processing*, 2014.

[27] 広田 修. INTERVIEW 民生有望技術：日本は何を? あらゆる悪天候下でも画像化できる量子レーダカメラとは. **防衛技術ジャーナル**, 36(11):12–17, 2016.

[28] Osamu Hirota. Importance and Applications of Infinite Dimensional Non-Orthogonal Quantum State. *Journal of Lasers, Optics & Photonics*, 3(1):1–10, 2016.

[29] Ryuichi Tadano, Adithya Kumar Pediredla, and Ashok Veeraraghavan. Depth Selective Camera: A Direct, On-Chip, Programmable Technique for Depth Selectivity in Photography. In *Proceedings of IEEE International Conference on Computer Vision*, 2015.

[30] Jian Wang, Joseph Bartels, William Whittaker, Aswin C. Sankaranarayanan, and Srinivasa G. Narasimhan. Programmable Triangulation Light Curtains. In *Proceedings of European Conference on Computer Vision*, 2018.

[31] Guy Satat, Matthew Tancik, and Ramesh Raskar. Towards photography through realistic fog. In *Proceedings of IEEE International Conference on Computational Photography*, 2018.

[32] Wenzel Jakob. Mitsuba renderer, 2010. `http://www.mitsuba-renderer.org`.

[33] 安富 啓太, 川人 祥二. Time-of-Flight カメラ. **映像情報メディア学会誌**, 70(11):880–885, 2016.

[34] Melexis. Application note: Time-of-flight basics, 2017. `https://www.mouser.com/pdfdocs/Time-of-Flight-Basics-Application-Note-Melexis.pdf`.

Appendix

Appendix A: Analysis of phasor distortions

Modulation frequency: 100 kHz

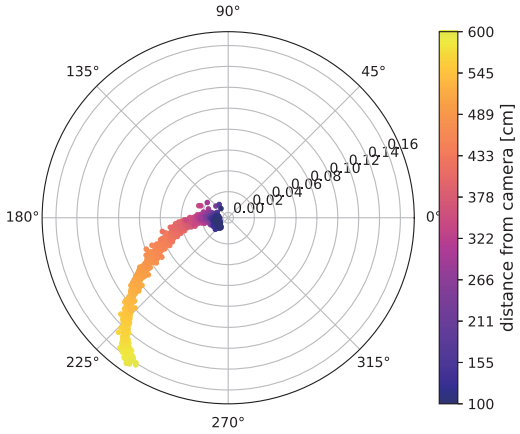

(a) Scattering coefficients 0.005: Measured value (scattered light + reflected light)

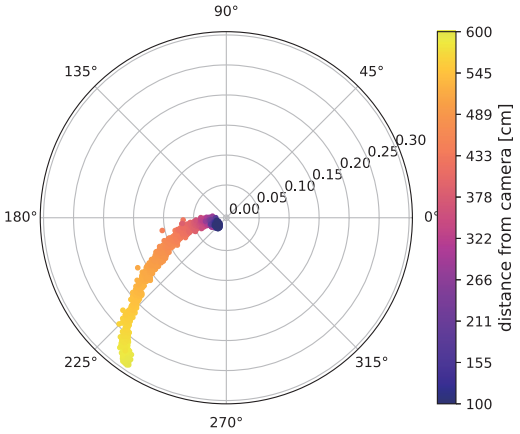

(b) Scattering coefficients 0.01: Measured value (scattered light + reflected light)

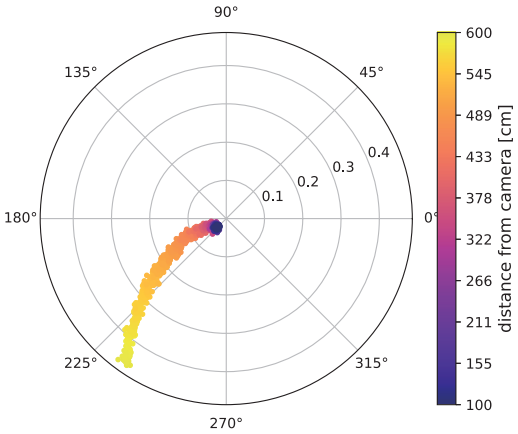

(c) Scattering coefficients 0.02: Measured value (scattered light + reflected light)

Figure 8.1: Phasor transition at modulation frequency of 100 kHz.

Modulation frequency: 200 kHz

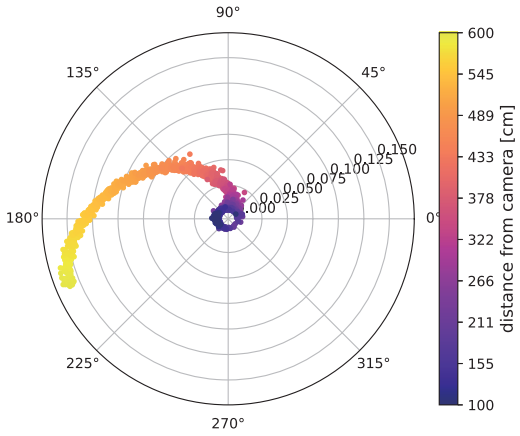

(a) Scattering coefficients 0.005: Measured value (scattered light + reflected light)

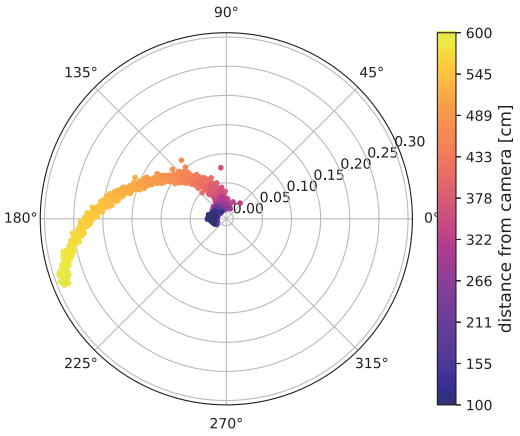

(b) Scattering coefficients 0.01: Measured value (scattered light + reflected light)

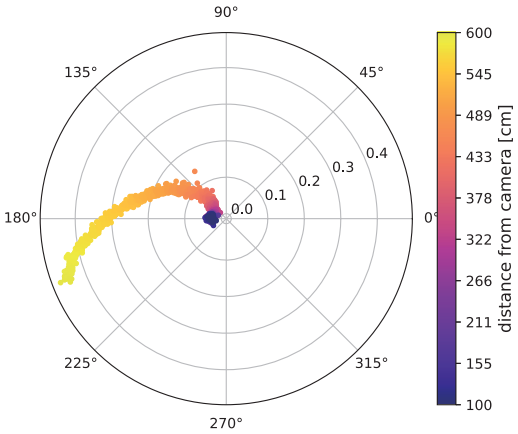

(c) Scattering coefficients 0.02: Measured value (scattered light + reflected light)

Figure 8.2: Phasor transition at modulation frequency of 200 kHz.

Modulation frequency: 300 kHz

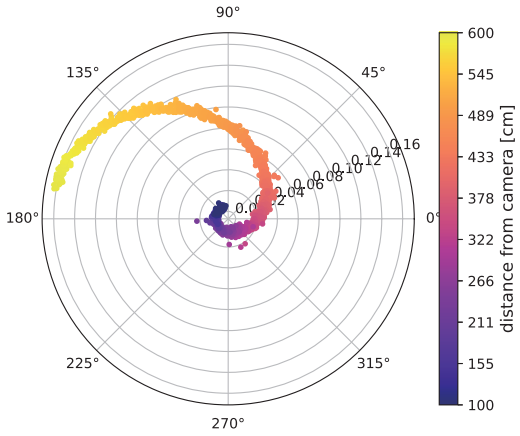

(a) Scattering coefficients 0.005: Measured value (scattered light + reflected light)

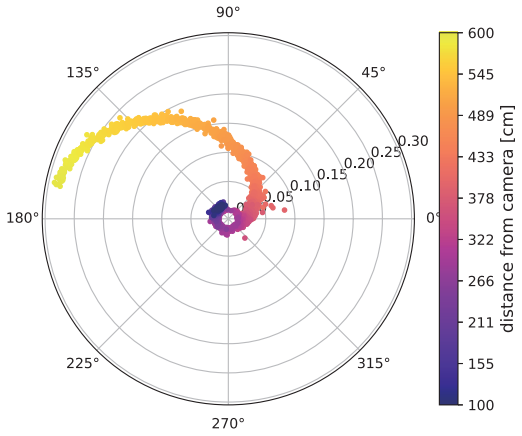

(b) Scattering coefficients 0.01: Measured value (scattered light + reflected light)

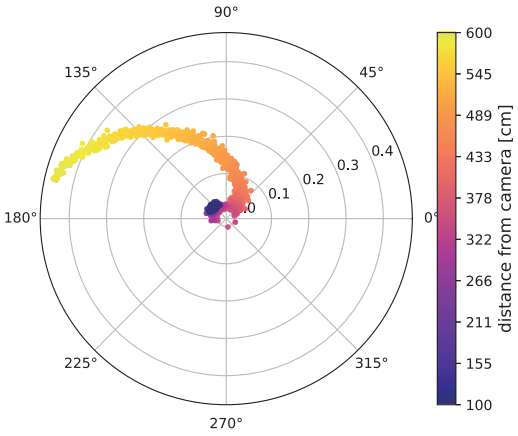

(c) Scattering coefficients 0.02: Measured value (scattered light + reflected light)

Figure 8.3: Phasor transition at modulation frequency of 300 kHz.

Modulation frequency: 400 kHz

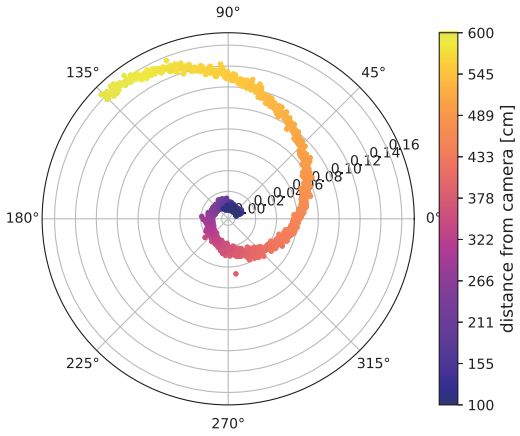

(a) Scattering coefficients 0.005: Measured value (scattered light + reflected light)

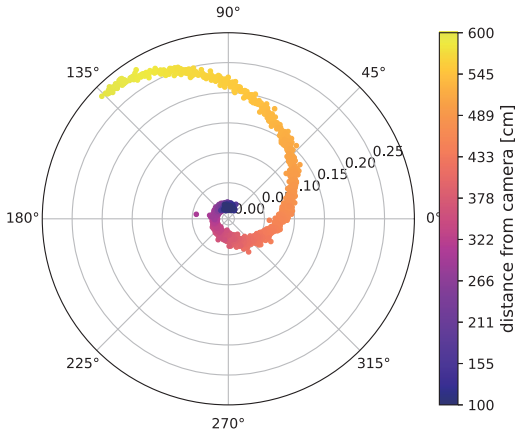

(b) Scattering coefficients 0.01: Measured value (scattered light + reflected light)

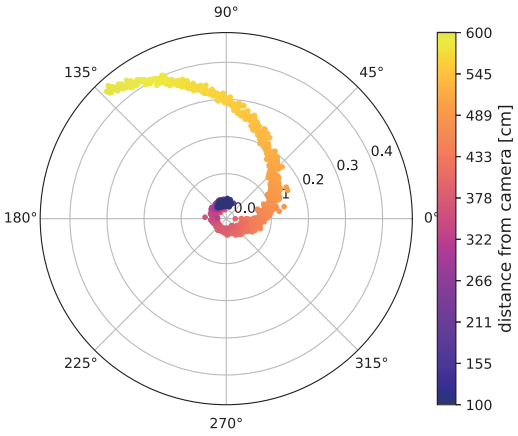

(c) Scattering coefficients 0.02: Measured value (scattered light + reflected light)

Figure 8.4: Phasor transition at modulation frequency of 400 kHz.

Modulation frequency: 500 kHz

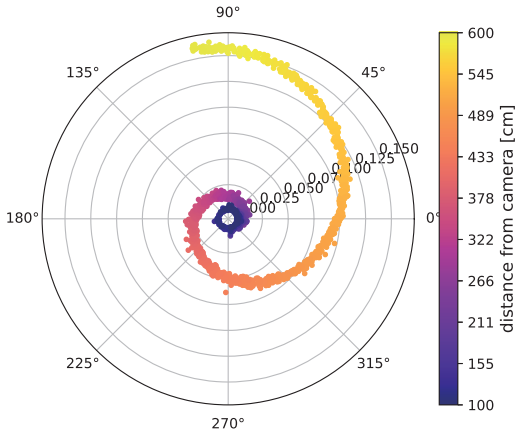

(a) Scattering coefficients 0.005: Measured value (scattered light + reflected light)

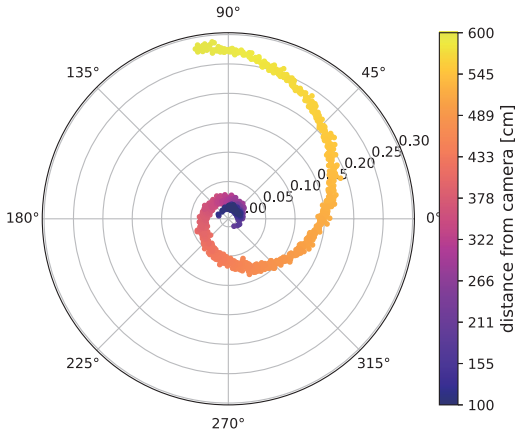

(b) Scattering coefficients 0.01: Measured value (scattered light + reflected light)

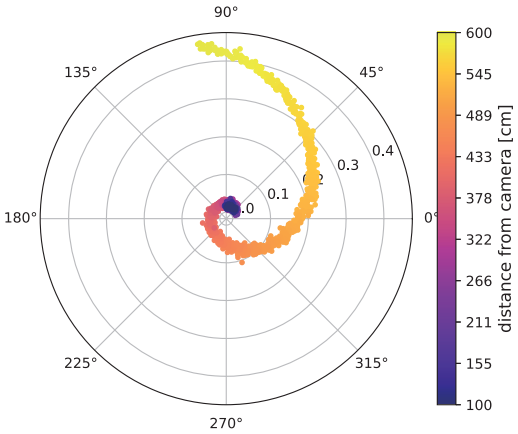

(c) Scattering coefficients 0.02: Measured value (scattered light + reflected light)

Figure 8.5: Phasor transition at modulation frequency of 500 kHz.

Modulation frequency: 600 kHz

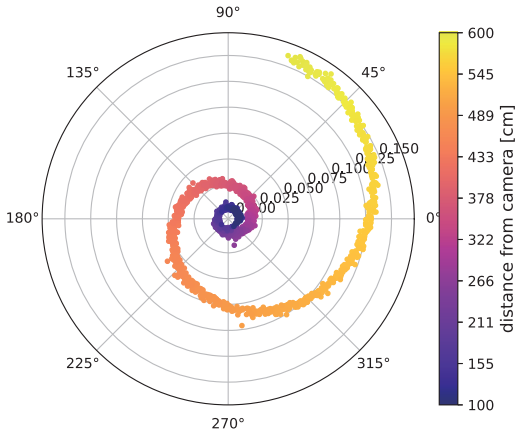

(a) Scattering coefficients 0.005: Measured value (scattered light + reflected light)

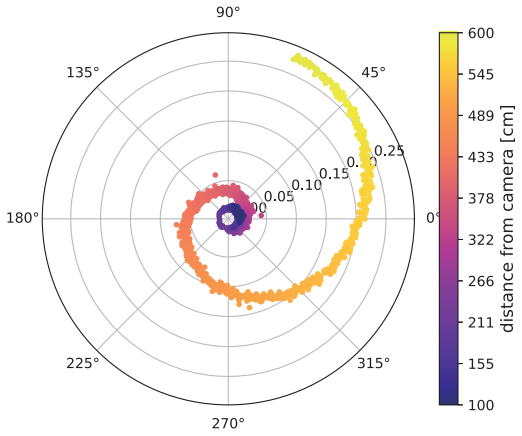

(b) Scattering coefficients 0.01: Measured value (scattered light + reflected light)

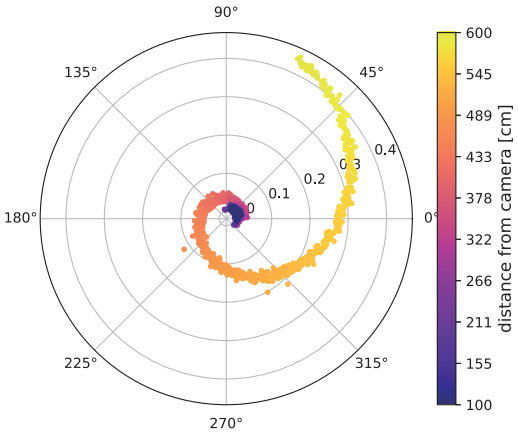

(c) Scattering coefficients 0.02: Measured value (scattered light + reflected light)

Figure 8.6: Phasor transition at modulation frequency of 600 kHz.

Modulation frequency: 700 kHz

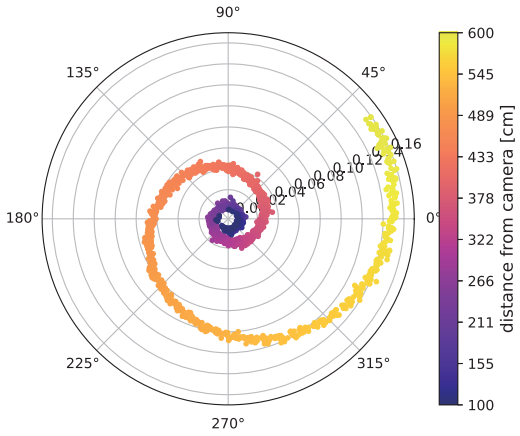

(a) Scattering coefficients 0.005: Measured value (scattered light + reflected light)

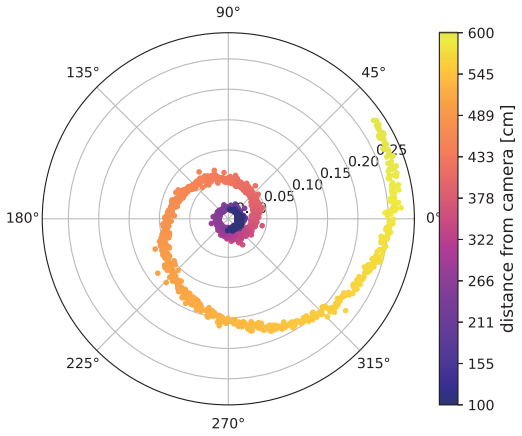

(b) Scattering coefficients 0.01: Measured value (scattered light + reflected light)

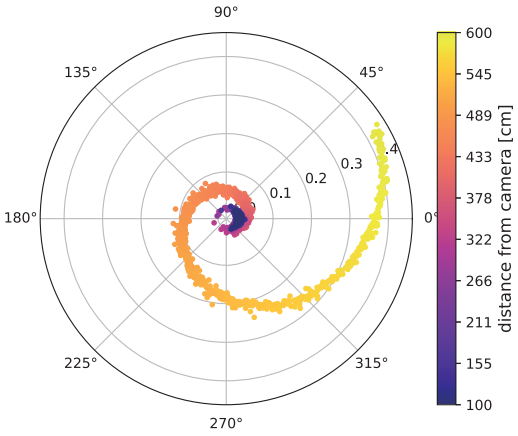

(c) Scattering coefficients 0.02: Measured value (scattered light + reflected light)

Figure 8.7: Phasor transition at modulation frequency of 700 kHz.

Modulation frequency: 800 kHz

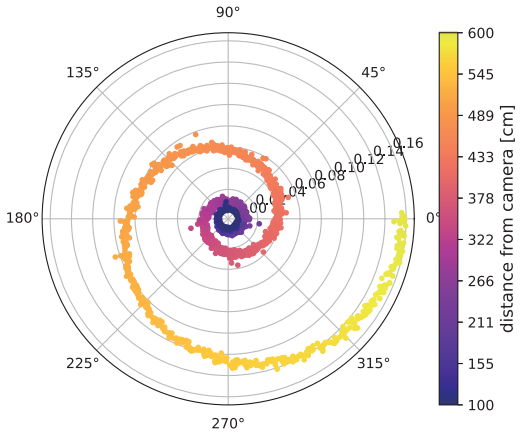

(a) Scattering coefficients 0.005: Measured value (scattered light + reflected light)

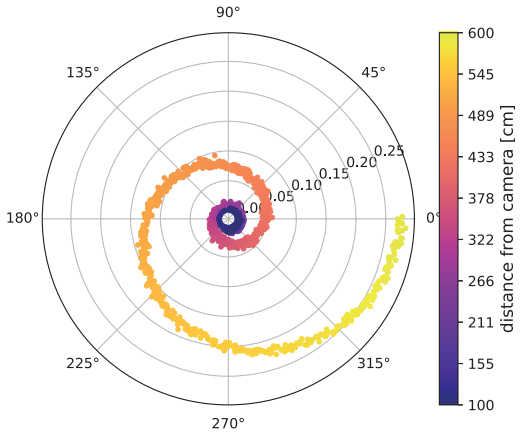

(b) Scattering coefficients 0.01: Measured value (scattered light + reflected light)

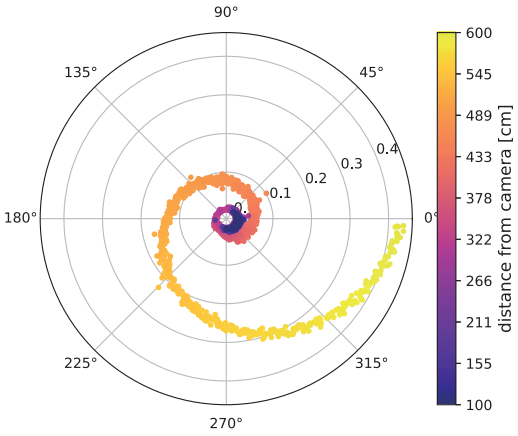

(c) Scattering coefficients 0.02: Measured value (scattered light + reflected light)

Figure 8.8: Phasor transition at modulation frequency of 800 kHz.

Modulation frequency: 900 kHz

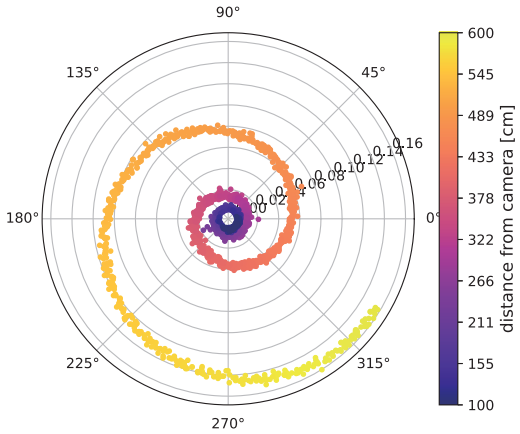

(a) Scattering coefficients 0.005: Measured value (scattered light + reflected light)

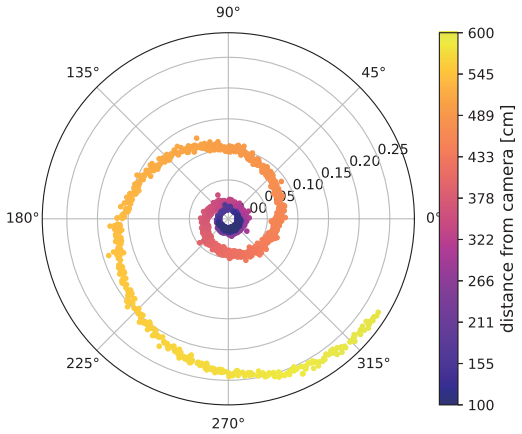

(b) Scattering coefficients 0.01: Measured value (scattered light + reflected light)

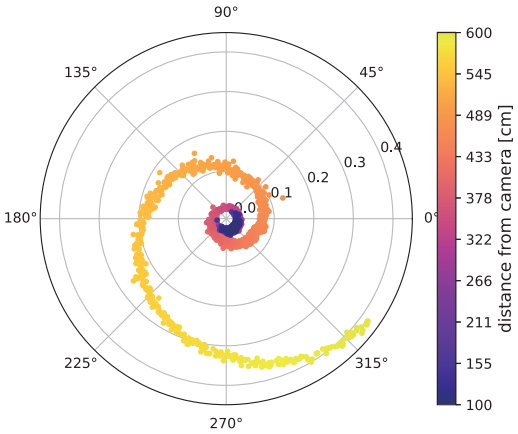

(c) Scattering coefficients 0.02: Measured value (scattered light + reflected light)

Figure 8.9: Phasor transition at modulation frequency of 900 kHz.

Modulation frequency: 1 MHz

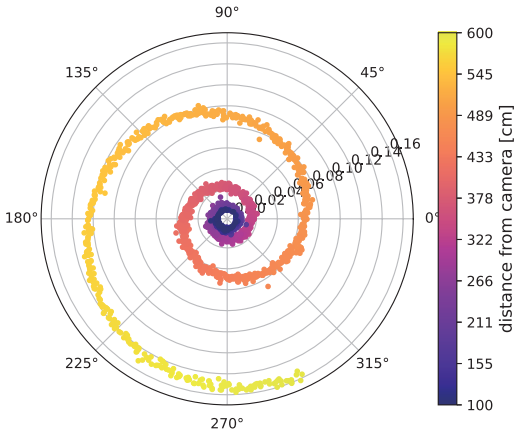

(a) Scattering coefficients 0.005: Measured value (scattered light + reflected light)

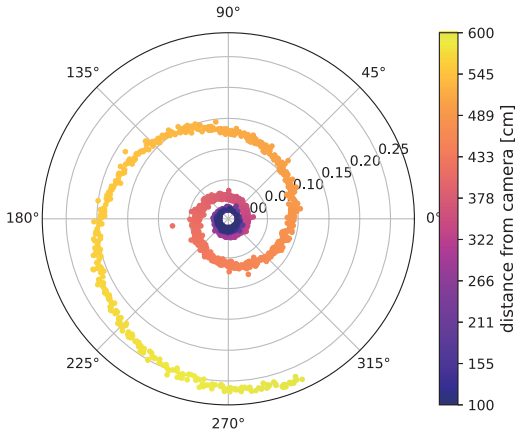

(b) Scattering coefficients 0.01: Measured value (scattered light + reflected light)

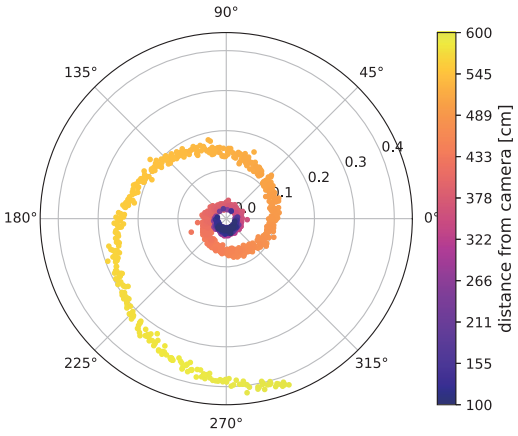

(c) Scattering coefficients 0.02: Measured value (scattered light + reflected light)

Figure 8.10: Phasor transition at modulation frequency of 1 MHz.